1

A long-term, high-latitude record of Eocene hydrological change in the Greenland region

4

5 Gordon N. Inglis [1,2], Matthew J. Carmichael [1,2,3], Alex Farnsworth [2,3], Daniel J.

6 Lunt [2,3] and Richard D. Pancost [1,2]

7

8 (1) Organic Geochemistry Unit, School of Chemistry and School of Earth

9 Science, University of Bristol, UK

10 (2) Cabot Institute, University of Bristol, UK

11 (3) BRIDGE, School of Geographical Sciences, University of Bristol, UK

12

13 Corresponding author: Gordon N. Inglis

14

15 Email: gordon.inglis@bristol.ac.uk. Telephone: +44 (0)117 954 6395

16

17

18

19

20

21

22

23   **Abstract.**

24   A range of proxy approaches have been used to reconstruct short-term changes to

25   Earth's hydrological cycle during the early Eocene hyperthermals. However, little is

26   known about the response of Earth's hydrological and biogeochemical systems to

27   long-term Cenozoic cooling, which began following the Early Eocene Climatic

28   Optimum (53.3 – 49.4 million years ago; Ma). Here, we use the molecular distribution

29   and isotopic composition of terrestrial biomarkers preserved in marine sediments of

30   ODP Site 913, East Greenland, to develop a long-term record of high-latitude

31   hydrological change between 50 and 34 Ma. There is a marked decline in the

32   concentration of conifer-derived diterpenoids and angiosperm-derived triterpenoids

33   during the Eocene. As the input of wind-blown conifer pollen remains stable during this

34   interval, this implies that decreasing di- and triterpenoid concentrations reflect

35   declining influence of fluvial inputs – and perhaps terrestrial runoff – throughout the

36   Eocene. Branched GDGTs and bacterial-derived hopanes indicate an increased input

37   of soil- and kerogen-derived organic matter, respectively, after 38 Ma. This coincides

38   with evidence for ice rafted debris and suggests input of organic matter via glacial

39   processes. This also implies some continental glaciation occurred in the middle-to-

40   late Eocene. Leaf wax hydrogen isotopes extending throughout this section – the first

41   such long-term record from the Paleogene - indicate that precipitation δ^2H was

42   persistently higher than that of modern coastal Greenland, consistent with warmer

43   ocean source waters and enhanced poleward moisture transport. Non-intuitively,

44   however, this effect appears to have been smallest during the warmest part of the

45   record, and higher δ^2H values occur in the middle Eocene. Although interpretation of

46   these hydrogen isotope trends is unclear, they clearly indicate – alongside the

47   changes in biomarker abundances – a perturbed hydrological cycle through the

48 Eocene in coastal Greenland. More long-term records are required to ascertain if this

49 represents regional or global hydrological reorganisation.

50

51 **Keywords**: biomarkers; alkanes; vegetation; Cenozoic; Palaeogene

52

53 **1. Introduction**

54 Past greenhouse climates can provide insights into how the Earth's hydrological cycle

55 differed during intervals of global warmth. Several previous studies have focused upon

56 the Paleocene-Eocene Thermal Maximum (PETM; ~56 million years ago; Ma), a

57 hyperthermal event characterised by surface temperature warming of between 5 - 9

58 °C and a rapid onset of less than 20 kyr (Hollis et al., 2019; Kennett and Stott, 1991;

59 Sluijs et al., 2007; Sluijs et al., 2006; Tripati and Elderfield, 2005; Zachos et al., 2006;

60 Zachos et al., 2003). During this interval, the hydrological cycle appears to have been

61 particularly sensitive to warming (Carmichael et al., 2017; Carmichael et al., 2018) and

62 multi-proxy records provide evidence for increased high-latitude precipitation (Pagani

63 et al., 2006; Sluijs et al., 2008). In addition, a range of mid-high latitude records indicate

64 increased continental runoff, including in the North Sea (Kender et al., 2012), Svalbard

65 (Dypvik et al., 2011) and New Zealand (Crouch et al., 2003). Recent studies have

66 indicated that the subsequent Eocene hyperthermals, including Eocene Thermal

67 Maximum 2, were also associated with changes in the hydrological cycle (Krishnan et

68 al., 2014).

69   A range of PETM studies have utilised the hydrogen isotopic composition (δ^2H)

70 of lipid biomarkers, of presumed leaf-wax origin, to reconstruct hydrological responses

71 within the PETM (Garel et al., 2013; Handley et al., 2012; Pagani et al., 2006; Smith

72 et al., 2007; Tipple et al., 2011) and of the later Eocene hyperthermals (Krishnan et

73   al., 2014). However, a number of these records span only the time period immediately

74   before or after the PETM carbon isotope excursion (CIE). In addition, some of the

75   measured sections suffer from unconformities, preventing an assessment of whether

76   δ^2H values returned to pre-event values (Handley et al., 2012), whilst others show

77   evidence for significant hydrological perturbations ahead of the onset of the CIE (Garel

78   et al., 2013; Handley et al., 2011). Therefore, to contextualise these responses, longer-

79   term assessments of changes in hydrology are required.

80   Moreover, the sensitivity of the hydrological cycle to longer-term Eocene

81   temperature trends remains largely unexplored. Although the multi-million-year

82   sustained warmth of the EECO (53.3 – 49.4 Ma) appears to have been associated

83   with an intensified hydrological cycle relative to preindustrial conditions (Carmichael

84   et al., 2016) this interpretation is based on relatively few records and the response of

85   the hydrological cycle to long-term middle and late Eocene cooling remains unknown.

86   This is crucial as the hydrological cycle is likely to have been important in regulating

87   Earth's climate over long timescales, for example, through changes in atmospheric

88   latitudinal heat transport (Pierrehumbert, 2002) and continental weathering (Beaulieu

89   et al., 2012). Such changes will also impact marine productivity (Kelly et al., 2005) and

90   possibly ocean circulation via changes in the distribution of precipitation and

91   evaporation (Bice and Marotzke, 2002). Long term, multi-proxy records are therefore

92   critical to understanding the relative importance of these processes throughout the

93   Cenozoic.

94   Here, we explore Eocene hydroclimatic changes within East Greenland by

95   analysing lipid biomarkers preserved within the sediments of Ocean Drilling Program

96   (ODP) Site 913B (Myhre et al., 1995). This site represents one of the best long-term

97   high-latitude records for Eocene environmental changes, with continuous deposition

98   having occurred from the EECO to the Eocene-Oligocene boundary (Schouten et al.,

99   2008). This interval coincides with a significant decrease in pCO$_2$ (Anagnostou et al.,

100   2016) and consequent global (Zachos et al., 2008) and regional (Bijl et al., 2009;

101   Cramwinckel et al., 2018; Inglis et al., 2015b) cooling, with TEX$_{86}$ data suggesting ca.

102   7°C of cooling between the EECO and late Eocene at the high latitudes (Inglis et al.,

103   2015). Given that high-latitude sites appear to have been hydrologically sensitive to

104   increased temperatures at the PETM (see Carmichael et al., 2017 and ref. therein), a

105   gradual reduction in precipitation and runoff is expected to be recorded at Site 913 in

106   response to the long-term regional cooling (c.f. Eldrett et al., 2009). To test this, we

107   analyse the distribution, concentration and isotopic composition of the diverse

108   terrestrial biomarkers within ODP Site 913 sediments and provide insights into a range

109   of paleoenvironmental processes around Greenland, including changes in vegetation

110   and fluvial, aeolian and glacial transport processes. The results are then integrated

111   with previously published data to yield insights into the environmental changes

112   impacting the drill site throughout the Eocene. The results are then interpreted in the

113   context of a suite of climate model simulations to assist in the elucidation of complex

114   and multiple environmental controls, and to test and compare competing hypotheses.

115

116   **2. Methods**

117   **2.1. Site description**

118   Ocean Drilling Program (ODP) Leg 151 Site 913 (Myhre et al., 1995), located in the

119   Norwegian-Greenland Sea (75° 29' N, 6 ° 57' W, water depth, ~3300 m), was drilled

120   in September 1993. The site was deposited in a slope or basinal setting and offers

121   near continuous deposition between the Early Eocene and Eocene-Oligocene

122   boundary (Eldrett et al., 2007; Schouten et al., 2008). Based on the age model of

123   Eldrett et al. (2009) and updated by Inglis et al. (2015), the samples studied in this

124   paper span the interval 50 Ma to 34 Ma. During the earliest Eocene, the Norwegian

125   Greenland Sea consisted of a series of highly restricted embayments (Figure 1), which

126   were subject to stepwise tectonic opening throughout the Eocene (Hohbein et al.,

127   2013). Over the course of the Eocene, the location of the Site 913 drill site likely

128   migrated northwards, from around 65°N during the early Eocene to around 70°N by

129   the late Eocene (Supplementary Information).
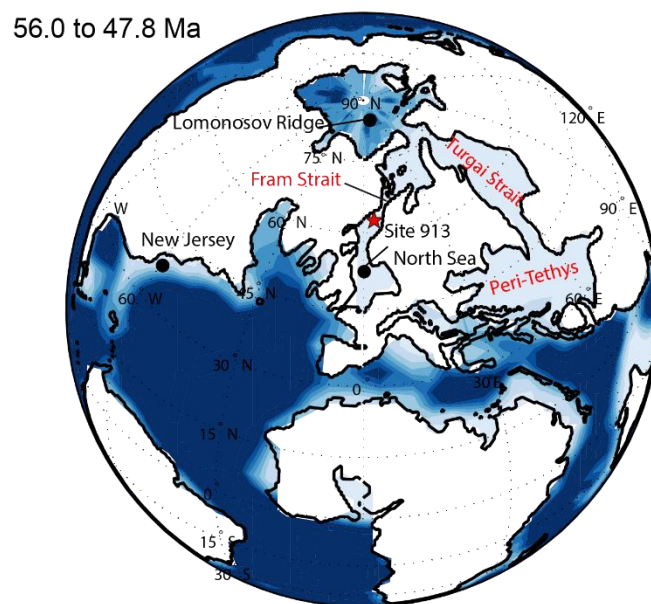
Figure 1. Location of ODP Site 913 during the Early Eocene (56 to 47.8 Ma; red star). Locations of other key Northern Hemisphere records are also shown (black points). Lighter blue shading indicates shallower water depths.

130   The lithology at Site 913 exhibits significant variation throughout the section

131   (Firth et al., 1995; Myhre et al., 1996). Lithological Unit 4 (ca. 674 to 770 mbsf)

132   deposited before 48 Ma, shows lamination and comprises massive silty clays and silty

133   muds. At just below 702 mbsf (~49.1 Ma), millimetre-sized coal fragments are

134   observed. These sediments are assumed to have been deposited close to the paleo-

135   shoreline and under the influence of gravity flows (Myhre et al., 1995; Thiede and

136   Myhre, 1996). Unit 3 sediments (< 674 mbsf, deposited after 48 Ma) comprise primarily

137   clays, with biosiliceous clays dominant between ca. 462 and 500 mbsf (37 - 39 Ma).

138   Unit 3 sediments are suggested to have been deposited under lower energy currents

139   with a greater influence of aeolian transport (Myhre et al., 1995; Thiede and Myhre,

140   1996).

141

142   **2.2. Organic geochemistry**

143   A total of 32 sediments from ODP Site 913B, comprising Unit 4 and Unit 3 sediments,

144   ranging in age from ~34 to ~50 Ma, were freeze-dried and exterior surfaces rinsed in

145   dichloromethane (DCM):Methanol (MeOH) (2:1 v/v) to remove surface contaminants

146   before powdering in a Retsch planetary ball mill. Between 25 and 30 g of each

147   sediment was subsequently extracted via Soxhlet apparatus for 24 hours using

148   DCM:MeOH (2:1 v/v) as the organic solvent. Activated copper was added to each

149   sample to remove elemental sulphur following the extraction. The TLE was separated

150   by column chromatography with activated silica (230 - 400 mesh) using ammonium

151   saturated chloroform and chloroform:acetic acid (100:1 v/v) to elute a neutral fraction

152   and an acid fraction, respectively (modified from Dickson et al. 2009). An internal

153   standard consisting of 10 µl 5α-androstane was added to each sample to quantify GC-

154   amenable apolar compounds. The neutral fractions were subsequently separated into

155   apolar and polar fractions by alumina column chromatography (activity II, 150 mesh),

156   eluting with n-Hexane:DCM (9:1 v/v) and DCM:MeOH (1:2 v/v), respectively.

157   For samples with significant co-elution of other hydrocarbons between the

158   target n-alkane compounds, urea adduction was performed to separate cyclic and

159   acyclic compounds (Pancost et al., 2008). Urea saturated methanol (200µl) was added

160 to each sample, followed by acetone (200µl) and *n*-hexane (200µl). Samples were

161 frozen for 30 minutes to aid crystal formation and then dried under nitrogen flow. Urea

162 crystals were washed with *n*-hexane to remove the non-adducted cyclic and branched

163 compounds (e.g. terpenoids). To obtain the acyclic, unbranched compounds (e.g. *n*-

164 alkanes), the urea crystals were then dissolved in MeOH:double distilled water (DDW)

165 and extracted by washing with hexane.

166

167 **2.2.1. GC-MS analysis**

168 Apolar fractions were initially screened by gas chromatography flame ionisation

169 detection (GC-FID) to determine appropriate concentrations for subsequent analytical

170 analyses. Identification of biomarkers in the apolar fractions then proceeded by gas

171 chromatography mass spectrometry GC-MS analysis, using a ThermoQuest Trace

172 GC-MS fitted with 50 m x 0.32 mm i.d. fused silica column with HP1 stationary phase.

173 The GC oven program was as follows: starting temperature 70°C, rising at 20°C / min

174 to 130°C before rising at 4°C / min for 42.5 minutes resulting in a final temperature of

175 300°C. The oven temperature was then held stable for 20 minutes giving a total run-

176 time of 65.5 minutes. The electron ionisation source was set to 70 eV. Scanning

177 occurred in the range 50 to 650 *m/z*. Compounds were identified primarily by mass

178 spectra and comparison of relative retention times in existing literature.

179

180 **2.2.2. LC-MS analysis**

181 The polar fraction, containing the isoprenoidal and branched GDGTs, was dissolved

182 in hexane/*iso*-propanol (99:1, v/v) and passed through 0.45 µm

183 polytetrafluoroethylene (PTFE) filters. Fractions were analysed by high performance

184 liquid chromatography/atmospheric pressure chemical ionisation – mass spectrometry

185   (HPLC/APCI-MS). Samples were analysed to separate 5-methyl and 6-methyl

186   brGDGTs (Hopmans et al., 2016). Normal phase separation was achieved using two

187   Waters Acquity UPLC BEH Hilic (2.1 x 150 mm; 1.7 µm i.d.) with a flow rate of 0.2

188   ml.min^{-1}. Samples were eluted isocratically with 78% A and 18% B for 25 min followed

189   by a linear gradient to 35% B over 25 minutes, then a linear gradient to 100% B in 30

190   minutes, where A = hexane and B = hexane:IPA (9:1, v/v) (Hopmans et al., 2016). The

191   injection volume was 15 µL, typically from 100 µL. Analyses were performed using

192   selective ion monitoring mode (SIM) to increase sensitivity and reproducibility

193   (m/z 1302, 1300, 1298, 1296, 1294, 1292, 1050, 1048, 1046, 1036, 1034, 1032, 1022,

194   1020, 1018, 744, and 653).

195

196   **2.2.3. GC-C-IRMS analysis**

197   Compound specific hydrogen isotopic compositions were determined for C_{29} and C_{31}

198   n-alkanes by gas chromatography-combustion-isotope ratio mass spectrometry (GC-

199   C-IRMS) using a ThermoFisher Trace GC Ultra coupled to a ThermoFisher Scientific

200   Delta V Isotope Ratio MS. The GC column used was a 30 m x 0.25 mm i.d. fused silica

201   column with ZB1 stationary phase. The H_3-factor was measured daily allowing isotope

202   values to be corrected for protonation reactions occurring within the ion source of the

203   mass spectrometer (Sessions et al., 2001). The GC program was as follows: starting

204   temperature 70°C, rising at 10°C / min to 300°C, at which point the oven temperature

205   was held stable for 8 minutes, giving a total analysis-time of 32 minutes. Triplicate runs

206   of each sample were performed. The average error for a triplicate measurement was

207   typically < 5‰ (see Supplementary Information). Each individual sample was co-

208   injected with sacrificial compounds consisting of n-pentadecane and ethyl caprylate to

209   condition the reactor. Measured isotope values were normalised by comparing the

210 instrument's response to Schimmelmann standards consisting of a suite of 15 *n*-

211 alkanes (Sessions et al., 1999), injected before and after each triplicate of sample

212 runs. Normalised results are reported in standard per mil (‰) notation as δ^2H values

213 relative to Vienna Standard Mean Ocean Water (VSMOW) and calculated against

214 calibrated H_2 gas, introduced directly into the ion source.

215

216 **2.3. Biomarker proxies**

217 The distribution of branched glycerol dialkyl glycerol tetraethers (brGDGTs) in mineral

218 soils is influenced by mean annual air temperature (MAAT), with the degree of

219 methylation decreasing as temperature increases (De Jonge et al., 2014; Weijers et

220 al., 2007). This is captured in the methylation of branched tetraether (MBT'$_{5ME}$) index

221 (De Jonge et al., 2014; Naafs et al., 2017):

222 $\text{MBT'}_{5ME} = (\text{Ia} + \text{Ib} + \text{Ic}) / (\text{Ia} + \text{Ib} + \text{Ic} + \text{IIa} + \text{IIb} + \text{IIc} + \text{IIIa})$ (1)

223 For samples dominated by 5-methyl brGDGTs, MBT'$_{5ME}$ is translated to MAAT using

224 a revised mineral soil calibration (Naafs et al., 2017):

225 $\text{MAAT}_{soil}' = 39.09 \text{ x MBT'}_{5ME} - 14.40$ ($n = 177$, $R^2 = 0.76$, RMSE = 4.1 °C) (2)

226 Roman numerals refer to individual GDGT structures shown in the Supplementary

227 Information. In brief, I, II and III represent the tetra-, penta- and hexamethylated

228 components, respectively, and a, b and c represent the brGDGTs bearing 0, 1 or 2

229 cyclopentane moieties. 6-methyl brGDGTs are indicated by an apostrophe (e.g. IIa' –

230 see equation 4).

231 The distribution of isoprenoidal glycerol dialkyl glycerol tetraethers (isoGDGTs) in

232 marine sediments is influenced by sea surface temperature (SST), with the degree of

233   cyclisation increasing as temperature increases (Schouten et al., 2002). This is

234   captured in the tetraether index of 86 carbon atoms (TEX$_{86}$) index:

235   TEX$_{86}$ = (GDGT-2 + GDGT-3 + Crenarchaeol regioisomer) / (GDGT-1 + GDGT-2 +

236   GDGT-3 + Crenarchaeol regioisomer)   (3)

237   The numbers refer to individual GDGT structures shown in the Supplementary

238   Information. Here we correlate TEX$_{86}$ values to SST using the spatially-varying,

239   Bayesian regression model (BAYSPAR) (Tierney and Tingley, 2014b, 2015). This

240   calibration assumes a linear relationship with temperature. This approach does not

241   suffer from regression dilution bias (c.f. TEX$_{86}^{H}$; Kim et al., 2010) and provides a more

242   robust statistical framework for constraining uncertainty than the standard error

243   estimates of previous linear calibrations (Hollis et al., 2019; Tierney and Tingley,

244   2014a).

245   The ratio of branched GDGTs to crenarchaeol in marine sediments is a function

246   of organic matter input and is expressed as the Branched versus Isoprenoid Tetraether

247   (BIT) index (Hopmans et al., 2004):

248   BIT = (brGDGT-Ia + brGDGT-IIa(') + brGDGT-IIIa(')) / (brGDGT-Ia + brGDGT-IIa(') +

249   brGDGT-IIIa + Crenarchaeol)   (4)

250   The numbers refer to individual GDGT structures shown in the Supplementary

251   Information.

252   The average chain length (ACL) expresses the average number of carbon atoms

253   per molecule for the long-chain odd-carbon numbered *n*-alkanes (Pancost and Boot,

254   2004). The ACL is defined for *n*-alkanes using the following equation (Eglinton and

255   Hamilton, 1967):

256 ACL= (25 x C_{25}) + (27 x C_{27}) + (29 x C_{29}) + (31 x C_{31}) + (33 x C_{33}) / (25 + 27 + 29 + 31

257 + 33)   (5)

258   The carbon preference index (CPI) reflects the dominance of odd-carbon-

259 numbered relative to even-carbon-numbered homologues (Bray and Evans, 1961).

260 The CPI is defined using the following equation (Bray and Evans, 1961):

261 CPI = 0.5 x ((C_{25} + C_{27} + C_{29} + C_{31} / C_{26} + C_{28} + C_{30} + C_{32}) + (C_{27} + C_{29} + C_{31} + C_{33} /

262 C_{26} + C_{28} + C_{30} + C_{32}))   (6)

263   Submerged and floating macrophyte plants, as well as many mosses, exhibit a

264 maximum in *n*-alkane distribution at C_{23} or C_{25}, with a particularly high concentration

265 of these homologues occurring in peat bog-dwelling *Sphagnum* moss. The dominance

266 of mid-chain vs long-chain *n*-alkanes is captured in the pAq index and defined for *n*-

267 alkanes using the following equation (Ficken et al., 2000):

268 pAq= C_{23} + C_{25} / C_{23} + C_{25} + C_{29} + C_{31} (7)

269   The terrestrial-aquatic ratio reflects the dominance of short- vs long-chain *n*-

270 alkanes and is defined for *n*-alkanes using the following equation (Pancost and Boot,

271 2004):

272 TAR = C_{17} + C_{19} + C_{21} / C_{29} + C_{31} + C_{33} (8)

273 **2.4. Climate model simulations**

274 The climate simulations described in this paper were carried out using the coupled

275 atmosphere-ocean climate model HadCM3L. Simulations were performed at ×2 and

276 ×4 preindustrial atmospheric CO_2 concentrations (i.e. 560 and 1120 ppmv,

277 respectively; Farnsworth et al., *in revision*) for each stratigraphic stage of the Eocene.

278   The paleogeographies were developed from geological reconstructions by Getech Plc

279   (Ypresian, 56.0 - 47.8 Ma; Lutetian, 47.8 - 41.2 Ma; Bartonian, 41.2 - 37.8 Ma and

280   Priabonian, 37.8 – 34.0 Ma). The climate model, and the ×4 simulations, are identical

281   to those described in detail in Lunt et al. (2016), except that here they have been run

282   for longer (10,422 years here compared with 1,422 years), in order to approach more

283   closely to equilibrium. The ×2 simulations are branched off from the ×4 simulations

284   after 422 years and run for 10,000 years (Farnsworth et al., in revision). The only

285   difference between the simulation of each stage relative to another stage is the

286   prescribed paleogeography (see Figure S1 in Supp Info of Lunt et al., 2016) and the

287   solar constant (see Figure 2 of Lunt et al., 2016). The climate model used for the

288   simulations is very similar to the HadCM3LM2.1E model described and evaluated in

289   Valdes et al. (2017), except that we include a modification to the ozone profile to

290   ensure that the model does not develop a runaway warming at ×4 CO_2, as discussed

291   in Lunt et al. (2016).

292

293   **3. Results**

294   **3.1. Biomarker distributions and their interpretation**

295   **3.1.1. *n*-alkanes**

296   Long chain *n*-alkanes with a strong odd-over-even predominance (C_{27} - C_{35}) are

297   typically attributed to epicuticular waxes synthesised by vascular plants (Eglinton and

298   Hamilton, 1967). At ODP Site 913, sediments exhibit varying *n*-alkane distributions

299   (Figure 2), indicative of changing plant inputs. The terrestrial aquatic ratio (TAR), the

300   ratio between long chain *n*-alkanes and shorter chain homologues, is commonly used

301   as a proxy for the input of terrestrial plant matter relative to marine algae and

302   phytoplankton (Cranwell, 1982). Decreasing TARs at Site 913 indicate an increasing

303   proportion of terrestrial inputs in the younger sediments (Figure 3a).
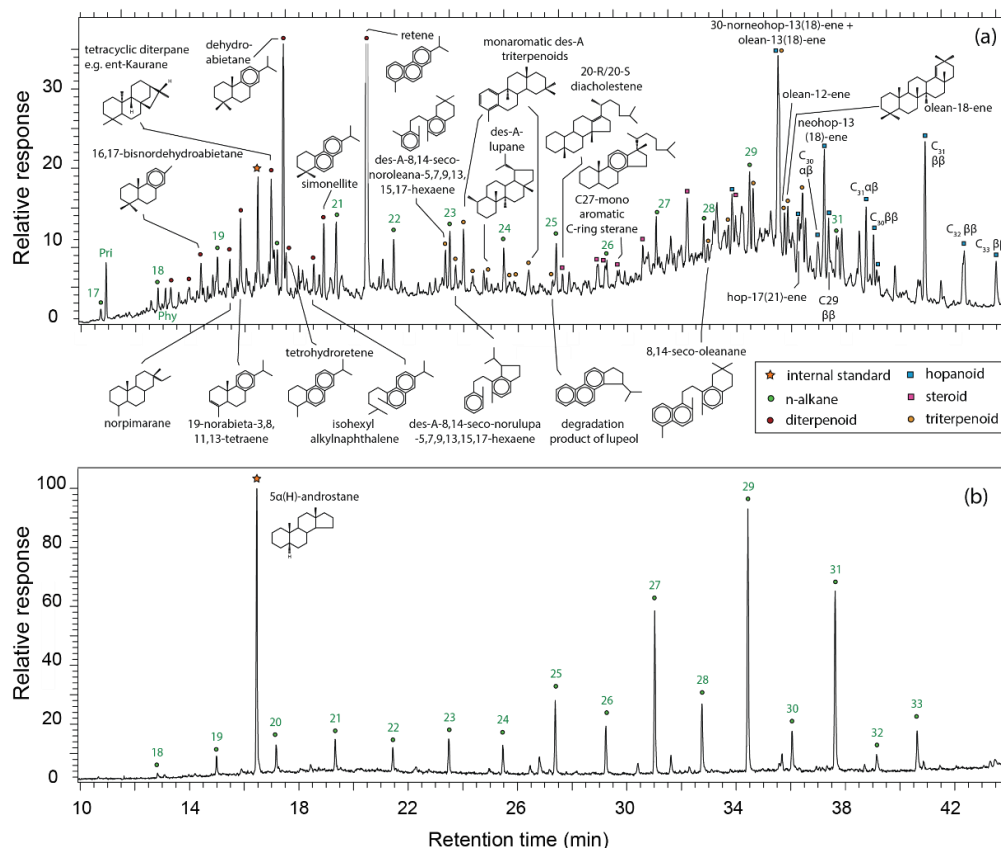
Figure 2: Diverse terrestrial biomarker distributions in ODP Site 913 sediments. Representative total ion current gas chromatograms shown for the (a) early Eocene (~49.2 Ma; 703.83 mbsf) and (b) late Eocene (~35.2 Ma; 464.31 mbsf). The structures of the principal plant-derived diterpenoids and triterpenoids and steroidal biomarkers are shown in (a). Numbers accompanied with Greek letters signify the carbon number and stereochemistry of hopanoids (a). Plant-derived *n*-alkanes are numbered according to the number of carbon atoms (a and b).
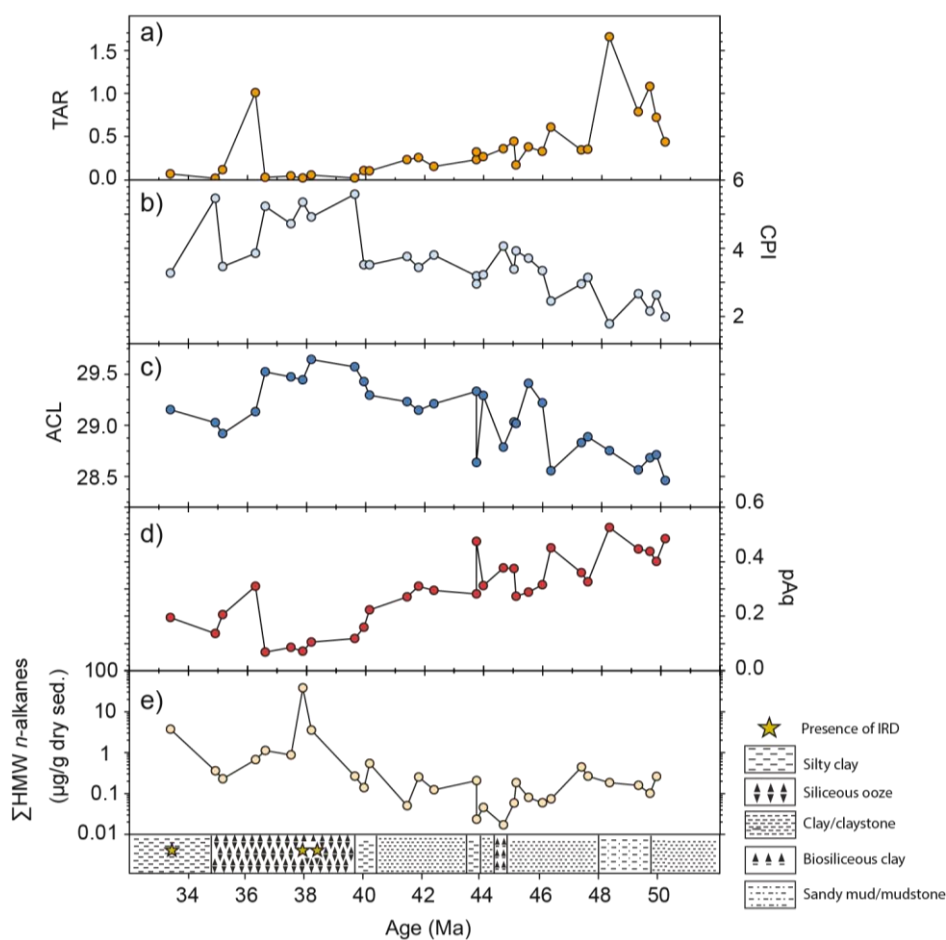
Figure 3: Input of plant-derived organic matter at ODP Site 913 during the Eocene; (a) carbon preference index (CPI); (b) average chain length (ACL), (c) P$_{aq}$ ratio, (d) terrestrial-aquatic ratio (TAR), (e) C_{27}-C_{33} *n*-alkanes (µg/g dry sediment). Also shown are the occurrences of dropstones (stars; Eldrett et al., 2004) and the changes in lithology (Myhrre et al., 1995). All data are updated to GTS2012.

304

305   Carbon preference indices (CPIs) in plant leaves are generally > 5 and

306   decrease during transport, degradation and thermal maturation (Diefendorf and

307   Freimuth, 2017). At Site 913, indices are typically > 2 throughout the section (Figure

308   3b), indicating thermally immature sediments which have retained the biological odd-

309   over-even predominance, consistent with a leaf wax origin. CPIs increase from ~2

310   during the early Eocene (~50 Ma) to ~3.5 during middle Eocene (~40 Ma), followed by

311   a further increase to higher, more variable values after 40 Ma (Figure 3b). Combined,

312   TARs (Fig. 3a) and CPIs (Fig. 3b) indicate a persistent but increasing input of minimally

313   degraded leaf waxes during the middle and late Eocene.

314   Other aspects of the *n*-alkane distribution can reveal insights into changing

315   vegetation sources. For example, the ACL (Figure 3c) exhibits values (ca. 28.5 to 29.5)

316   that are typical for terrestrial higher plants (ca. 27 to 30; Bush and McInerney, 2013;

317   Diefendorf et al., 2011; Diefendorf and Freimuth, 2017). The P_{aq} index – which has

318   previously been used to infer input of *Sphagnum* moss and/or aquatic plant species to

319   Eocene-aged sediments (Inglis et al., 2015a) - declines from values of ~0.5 in the

320   Early Eocene to values <0.1 in the late Eocene (Figure 3d), indicating a decline in

321   moss or aquatic plant species or an increase in terrestrial higher plants during the

322   Eocene.

323

324   **3.1.2. Diterpenoids**

325   Diterpenoids are principal constituents of higher plant resins and support tissues,

326   particularly in gymnosperms (Diefendorf et al., 2012; Simoneit et al., 1986). A range

327   of aromatic diterpenoid hydrocarbons occur in the oldest ODP Site 913 sediments (Fig.

328   2a), including retene (*m/z* 219), simonellite (*m/z* 237), 18- and 19-norabieta-8,11,13-

329   triene (*m/z* 241), tetrohydroretene isomers (*m/z* 223), and dehydroabietane and

330   methyl-dehydroabietane (*m/z* 255). These biomarkers have been widely attributed to

331   conifers in previous studies (e.g. Otto and Simoneit, 2001). Although minor

332   concentrations can be present within marine organisms (e.g. Lin and Chang, 2000),

333   such a source seems unlikely here where they dominate over algal biomarkers. The

334   concentrations and relative abundances of retene and simonellite decline markedly

335   between 49 Ma and 46 Ma and remain low throughout the middle to late Eocene

336   (Figure 4a - note that the scale is logarithmic).
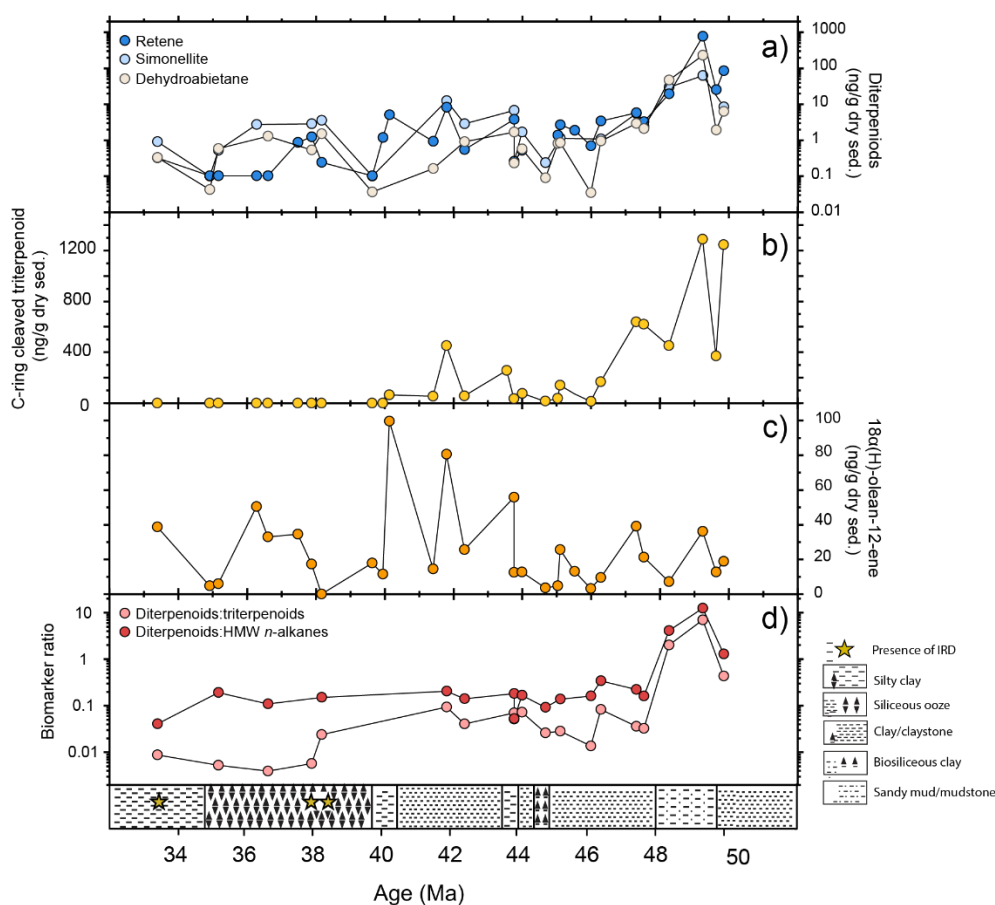
Figure 4: Input of gymnosperm- and angiosperm-derived biomarkers at ODP Site 913. (a) gymnosperm-derived diterpenoids (ng/g dry sediment) (retene - dark blue, simonellite - light blue, dehydroabietane - grey) (b) angiosperm-derived C-ring cleaved triterpenoid (ng/g dry sediment), (c) angiosperm-derived 18α(H)-olean-12-ene (ng/g dry sediment), (d) diterpenoids (summed retene, simonellite and dehydroabietane) relative to triterpenoids (18α(H)-olean-12-ene – light red) and long-chain n-alkanes (C_{27}, C_{29} and C_{31} n-alkanes – dark red).

337

3.1.3. Triterpenoids

339   Oleanoids, ursanoids and lupanoids are common triterpenoids in higher plants and

340   can trace terrestrial inputs within marginal marine settings (Rullkötter et al., 1994). Site

341 ODP 913 sediments, especially those from the middle Eocene, contain abundant

342 unsaturated oleanoids, including 18-α-(H)-olean-12-ene (Fig. 4c), olean-18-ene and

343 olean-13(18)-ene. The early and middle Eocene intervals also contain a variety of

344 degraded and aromatised triterpenoids, including C-ring cleaved aromatic

345 triterpenoids (Fig. 4b; de Las Heras et al., 1991) and des-A-triterpenoids (Jacob et al.,

346 2007; Fig. 2). All of the identified compounds derive from the oleanane and lupane

347 families, which are biomarkers of angiosperm plants and are diagenetic products of

348 oleanoic acids and β-amyrin (Rullkötter et al., 1994).

349 Given the differing principal origins of higher plant di- and triterpenoids, their

350 relative contributions have been used to assess changes in the composition of the

351 source vegetation (Bechtel et al., 2003; e.g. Fig. 4d). Whilst these changes are non-

352 quantitative - due to differences in lipid production between angiosperms and

353 gymnosperms (Diefendorf et al., 2014) and differing effects of diagenesis on different

354 compounds (Nakamura et al., 2010) - they suggest a relative decline in the input of

355 diterpenoids relative to triterpenoids at Site 913, with a marked change at about 48 Ma

356 (Fig. 4d). A similar result is obtained when normalising diterpenoids to long-chain *n*-

357 alkanes (Fig. 4d). Overall, the high abundances of a range of higher plant biomarkers

358 indicate a strong but changing terrestrial organic matter signal in the early Eocene.

359

360 **3.1.4. Hopanoids**

361 The apolar fractions contain a range of C_{27} - C_{34} hopanoids, including regular hopanes,

362 hopenes, benzohopanes and neohopenes (Figure 2a). These triterpenoids, especially

363 those > C_{30}, generally derive from bacteriohopanepolyols, which function as

364 membrane lipids in Bacteria (Sáenz et al., 2015; Talbot and Farrimond, 2007). hanges

365 in hopane stereochemistry occur during diagenesis and can be used to evaluate

366   changes in sediment thermal maturity (Mackenzie et al., 1980). With increasing

367   maturation, the 17β,21β configuration is transformed to the more stable 17β,21α(H)

368   and 17α,21β(H) configuration, although there are exceptions (Inglis et al., 2018). In

369   the extended C_{31} - C_{35} hopanes, a chiral centre also exists at the C22 position, which

370   racemizes during thermal maturation to form a mixture of 22S and 22R isomers

371   (Mackenzie et al., 1980). Such changes have been widely used to reconstruct the

372   thermal history of sediments, where decreasing ββ/(αβ + ββ) indices and increasing

373   22S/(22R + 22S) values indicate increasing thermal maturity. In general, both indices

374   at ODP Site 913 show the same trend: minimal variability and generally low, thermally

375   immature OM between 50 and 40 Ma that unexpectedly increases to more thermally

376   mature OM in the younger sediments (Fig. 5). In fact, hopanes in the biological

377   17β,21β(H) configuration are nearly absent in the youngest sediments (Fig. 5a), and

378   22S/(22S+22R) ratios, although more uncertain due to lower abundances and

379   coelution in some samples, decrease to near equilibrium values (0.3; Fig. 5b),

380   indicating high thermal maturity.

381

382   **3.1.5. Branched GDGTs**

383   Branched GDGTs derive predominantly from as-yet undetermined soil bacteria

384   (although acidobacteria are a likely source; Sinninghe Damsté et al., 2018). At ODP

385   Site 913, their distribution is dominated by tetramethylated brGDGTs (~54% of total

386   brGDGT distribution) and the abundance of 6-methyl brGDGT isomers is low-to-

387   moderate (~13% of the total brGDGT distribution). The low fractional abundance of 6-

388   methyl isomers can be attributed to 1) the dominance of tetramethylated brGDGTs

389   (which do not have a methyl group at the C-5 or C-6 position) and/or 2) a relatively

390   acidic depositional environment.
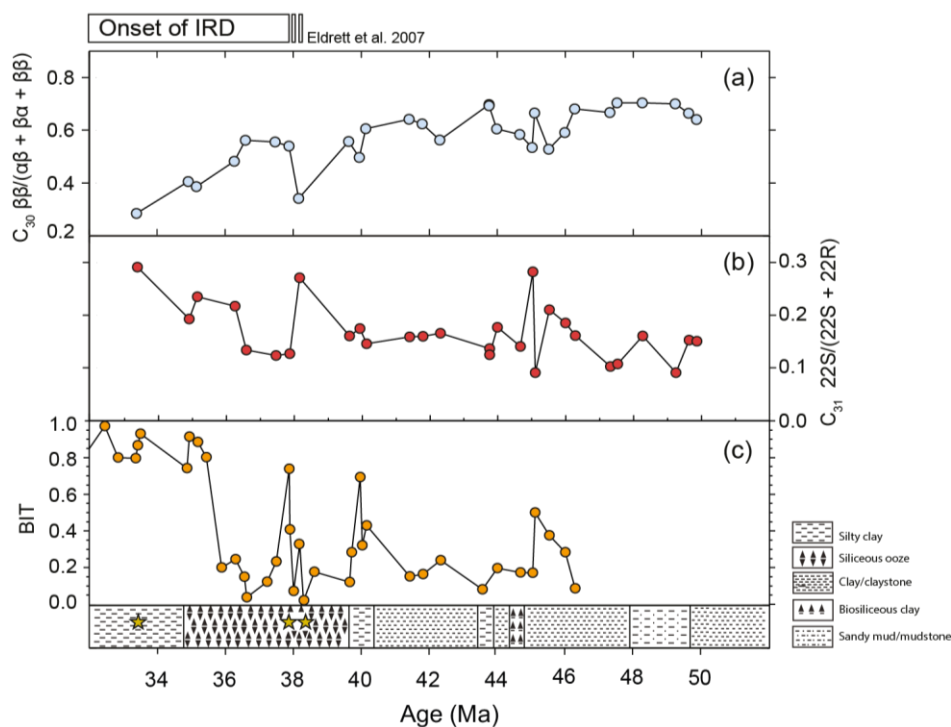
Figure 5: Input of soil- and kerogen-derived organic matter at ODP Site 913.

a) C_{30} hopane $\beta\beta/(\alpha\beta + \beta\beta)$ indices, (b) C_{31} hopane $22s/(22s + 22R)$ indices, (c) BIT index (Schouten et al. 2008, Liu et al. 2009, Inglis et al., 2015). Also shown are the occurrences of dropstones (stars; Eldrett et al., 2004), the changes in lithology (Myhrre et al., 1995) and approximate onset of IRD in ODP Site 913 sediments (Eldrett et al., 2007).

391   BIT indices have been previously reported for Site 913 from 40 - 31 Ma

392   (Schouten et al., 2008). That record exhibits no clear secular trend but does have great

393   variability, ranging between 0.17 (marine signal) to 0.98 (terrestrial signal) and

394   spanning nearly the entire range of the index (0 to 1). This was interpreted to reflect

395   variable inputs of terrestrial organic matter. Our new late Eocene data (Figure 5c) are

396   consistent with those of Schouten et al. (2008); where adjacent sediment samples

397   from the same core have been analysed, reproducibility of the BIT index is generally

398   strong (Supplementary Information). We also extend the existing BIT record with

399   sediments from the early - middle Eocene (Figure 5c), revealing a change in BIT

400   indices between 44 to 40 Ma. As reported by Schouten et al. (2008), younger

401   sediments, from 40 Ma and younger, have high and highly variable BIT indices, from

402   ~0.2 to greater than 0.9. However, sediments older than 44 Ma have markedly lower

403   BIT values and less variability, between 0.2 and 0.5 (Fig. 5c).

3.2. Hydrogen isotopic composition of *n*-alkanes

404

405   Further insight into the hydrological controls influencing ODP Site 913 sediments can

406   be obtained via compound specific hydrogen isotope analysis (δ^2H). The δ^2H value of

407   biomarkers, especially leaf waxes, have been used extensively to reconstruct the δ^2H

408   value of precipitation, providing insights into the operation of the past hydrological

409   cycle (Schefuß et al., 2005; Tierney et al., 2008; Tipple and Pagani, 2010). *n*-alkanes

410   are particularly suitable useful because hydrogen atoms are covalently bound to

411   carbon atoms, preventing isotopic exchange at temperatures below 100°C (Sachse et

412   al., 2012). The isotopic composition established during biosynthesis can therefore be

413   preserved over geological timescales, especially if they have experienced minimal

414   diagenetic or catagenetic alteration, as indicated for Site 913 *n*-alkanes by the

415   relatively high CPIs.

416   Changes in the hydrogen isotopic composition of C_{29} and C_{31} *n*-alkanes (δ^2H_{wax})

417   at ODP Site 913 are shown in Figure 6a. The C_{29} *n*-alkane is generally the most

418   abundant throughout the section (Fig. 6c), and its δ^2H values range between -229‰

419   and -154‰. The oldest samples, from the later stages of the EECO, have the most

420   ^2H-depleted values in the sequence, ca. -225‰. Between 48 and 46 Ma, progressive

421   deuterium enrichment occurs with decreasing age, reaching a maximum enrichment

422   at 45.5 Ma. In the middle Eocene, between 46 Ma and 42 Ma, δ^2H values remain

423   generally high, although there is some variability. From around 41 Ma to 33 Ma, δ^2H

424   values are relatively stable, varying between -185‰ and -205‰. The C_{31} *n*-alkanes

425   generally occur in lower abundances (Figure 6d), but reproducibility in their δ^2H values

426   is robust (Figure 6a; Supplementary Information) and the *n*-C_{31} δ^2H record is similar

427   to that of *n*-C_{29}, especially in the early and late Eocene. Intriguingly, between 46 Ma

428   and around 40 Ma, the δ^2H values of *n*-C_{29} and *n*-C_{31} are offset, with the latter failing

429   to record the excursion to particularly high δ^2H values recorded by the former. This

430   could arise from changes in leaf wax sources, and this is discussed below.
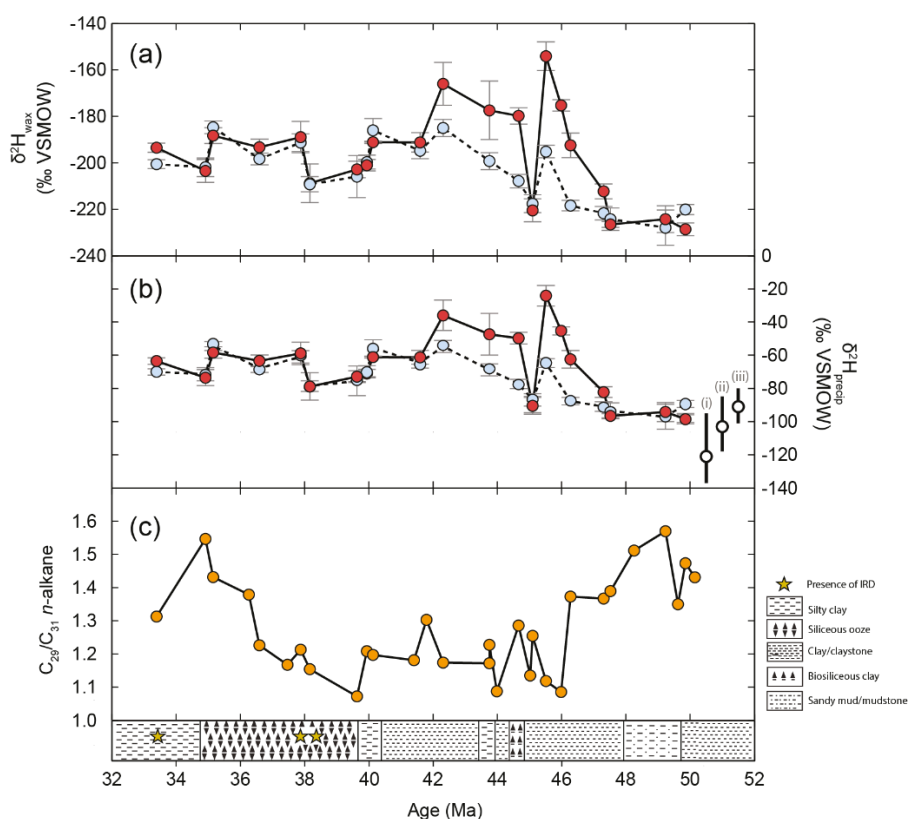
Figure 6: Leaf wax δ^2H values indicate a perturbed hydrological cycle on East Greenland during Eocene (a) δ^2H value of C_{29} (red) and C_{31} (blue) *n*-alkanes, (b) estimated δ^2H of precipitation (δ^2H_{precip}) assuming a net fractionation of -130‰. Also shown are estimates of modern-day δ^2H_{precip} on Greenland (see Table 1), (c) ratio of C_{29} to C_{31} *n*-alkanes. Also shown are the occurrences of dropstones (stars; Eldrett et al., 2004) and the changes in lithology (Myhrre et al., 1995).

431

432   **4. Discussion**

433   **4.1   High-latitude temperature change during the Eocene**

434   To investigate the influence of temperature change upon our terrestrial biomarker

435   distributions, we have compiled and developed new temperature estimates from ODP

436   Site 913 during the Eocene. Previously published branched GDGT-derived mean

437   annual air temperature (MAAT) estimates – assumed to reflect soil-derived GDGTs

438   delivered from Greenland – range between 12 and 18°C throughout the late Eocene

439   (39 to 34 Ma) with no obvious long-term trends (Schouten et al. 2008). However, that

440   study pre-dates the recent advances in analytical techniques that allow for the

441   separation of 5- and 6-methyl brGDGTs (Hopmans et al., 2016), and it did not utilise

442   the most recent calibrations (De Jonge et al., 2014; Naafs et al., 2017). Applying those

443   approaches, we have developed new branched GDGT-derived MAAT estimates in

444   ODP Site 913. Our results yield slightly lower MAAT estimates, ranging between ~12

445   and 16°C, throughout the middle and late Eocene (43 to 34 Ma; Fig. 7c); we could not

446   determine brGDGT-derived MAATs for the early Eocene due to the low abundance of

447   our target compounds. Our values are consistent with bioclimatic analyses (using the

448   Nearest Living Relative approach; Fig. 7a), which suggest relatively constant mean air

449   temperatures of around 14±3 °C throughout the middle and late Eocene (Eldrett et al.,

450   2009). Such bioclimatic analyses extend into the early Eocene, where they indicate

451   warm but surprisingly similar temperatures of~14°C (Fig. 7c).

452   Relatively stable terrestrial temperatures through the Eocene, especially into

453   the early Eocene (see Eldrett et al., 2009), are inconsistent with a changing vegetation

454   fossil pollen assemblage that indicates the presence of freshwater swamps, palms and

455   cycads during the early Eocene giving way to extensive coniferous forests during the

456   middle Eocene (Eldrett et al., 2009), under the influence of presumed long-term

457   cooling. To explore this mismatch, we compared our results alongside SST estimates

458   obtained from ODP Site 913 using TEX$_{86}$. Note that we have recalculated TEX$_{86}$-

459   derived SSTs from Inglis et al. (2015) using a spatially varying Bayesian calibration

460   (Tierney and Tingley, 2015). This approach indicates decreasing SSTs (ca. 6 to 8°C)

461   between 47 Ma and 34 Ma (Fig. 7d), consistent with the changing vegetation

462   assemblage (and global records) but contrasting with the stable temperatures

463   reconstructed using spore- and pollen-derived bioclimatic analysis.
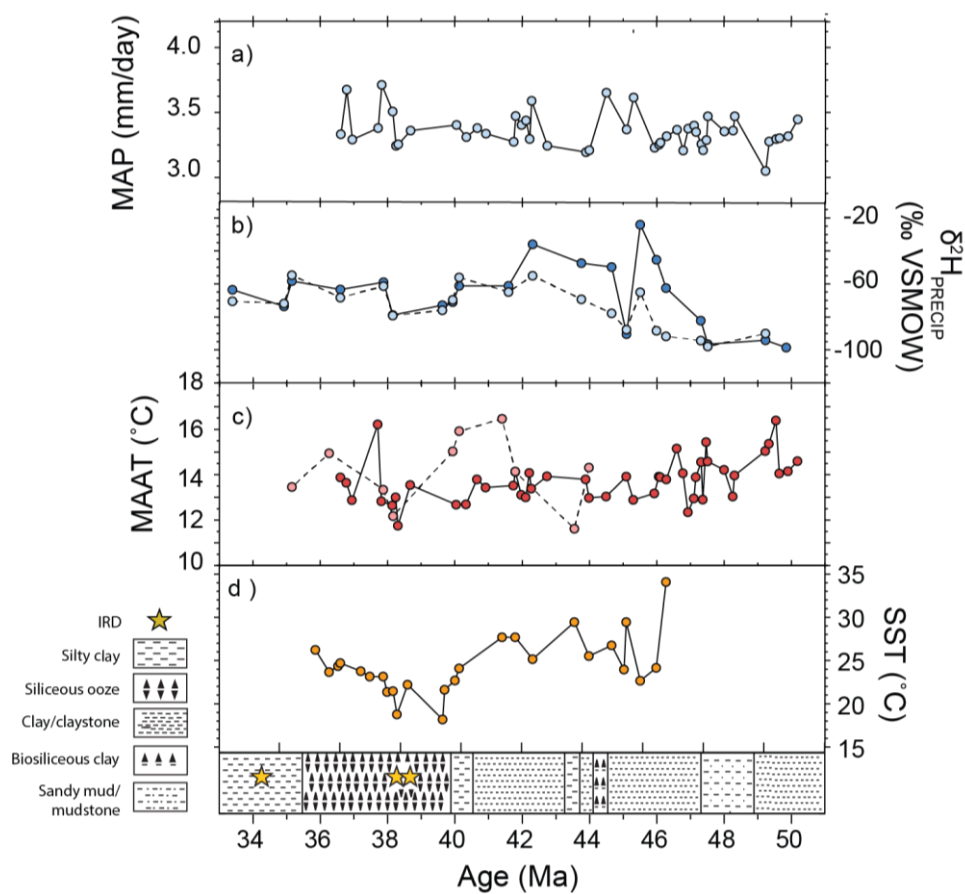
Figure 7: Temperature and hydrology on East Greenland during the Eocene;
a) MAP inferred from palynomorphs (Eldrett et al. 2009), b) δ^{2}H$_{precip}$ inferred from
leaf wax biomarkers (nC$_{29}$; dark blue, nC$_{31}$; light blue), c) MAAT inferred from
palynomorphs (Eldrett et al. 2009; dark red) and brGDGTs (light red), d) TEX$_{86}$-
derived SSTs. All data are updated to GTS2012.

464

465 **4.2   Controls on biomarker transport**

466 **4.2.1. Disentangling vegetation change and fluvial/aeolian mechanisms of**

467 **organic matter input**

468 Declining temperatures between the EECO and late Eocene are expected to impact

469 the hydrological cycle (Held and Soden, 2006). Previous interpretations, inferred from

470 ODP Site 913 pollen assemblages, indicates constant regional precipitation (Eldrett et

471 al., 2009), but we note that this approach also failed to identify declining SSTs (Inglis

472 et al., 2015b) or regional vegetation change (Eldrett et al., 2009). To probe

473 environmental conditions further, we utilise a range of biomarker ratios (e.g. TAR, pAq,

474 diterpenoids to triterpenoid ratios) to reconstruct changes in the sources of organic

475 matter and disentangle underlying transport mechanisms.

476   It is likely that decreasing terrestrial-to-aquatic ratios (TAR) during the middle

477 and late Eocene is driven by increasing aeolian and/or fluvial input of terrestrial-

478 derived higher plant leaf wax. This is consistent with the increase in long-chain *n*-

479 alkane concentrations, especially from 38 to 36 Ma (Fig. 3e) and decreasing P_{aq} values

480 (Fig. 3d). Intriguingly, the abundance of conifer-sourced diterpenoids decreases

481 markedly between the early and middle Eocene. These compounds – which can be

482 derived from leaves, resin and bark - are typically transported via river systems

483 (Medeiros et al., 2012; Medeiros and Simoneit, 2008), such that the trend suggests

484 decreasing fluvial inputs through time. Decreasing fluvial input is also consistent with

485 the long-term decrease in concentrations of angiosperm-derived triterpenoid

486 biomarkers (although that record is more complex; see below) and lower C/N ratios in

487 the middle and late Eocene (Andreasson et al., 1996). It is also consistent with

488 changes in lithology, which indicates fluvially-influenced sediments during the EECO

489 and more aeolian-deposited sediments in the middle Eocene (Myhre et al., 1995;

490 Thiede and Myhre, 1996). Seemingly in contradiction to this interpretation are the long-

491 term increase in BIT indices and the shift to more thermally mature hopane

492 distributions, and these are discussed below (see Section 4.2.2).

493   The difference between diterpenoid and *n*-alkane derived records, therefore,

494 likely arises from different transport processes governing their inputs, with the marked

495 decline in di- and triterpenoid concentrations (Figure 4a) reflecting weakening fluvial

496 inputs throughout the Eocene, and *n*-alkane abundances (Fig. 3e) and distributions

497 reflecting either stable or increasing aeolian inputs. The latter is consistent with the

498 input of wind-blown conifer pollen, which remains stable during this interval. Such an

499 explanation also accounts for the secular increase in CPIs, with *n*-alkanes in early

500 Eocene sediments likely reflecting degradation during storage and fluvial transport.

501 The qualitative interpretation of such organic matter source secular trends is

502 complicated by the multiple controls on fluvial and aeolian inputs (Pancost and Boot,

503 2004). The most important control is geography: in shelf and sometimes slope settings

504 and especially where close to river outflows, fluvial inputs dominate, whereas in the

505 open ocean beyond the influence of fluvial runoff, aeolian processes dominate

506 (Eglinton et al., 2002; Simoneit, 1977; Vogts et al., 2012). The magnitude of fluvial

507 inputs is also governed by intensity and nature of runoff, catchment dynamics, and

508 vegetation (Pancost and Boot, 2004), whereas aeolian inputs are governed by wind

509 strength and direction (i.e. see above papers).

510   Therefore, it is difficult to deconvolute the tectonic and climatic controls on the

511 decline in fluvial inputs. Below 550 m (prior to ~42.1 Ma), sediments are barren of

512 diatoms and the "common/abundant" classification is assigned only between 35 and

513 39 Ma (Scherer and Koç, 1996). Furthermore, the oldest diatoms at ODP Site 913 (ca.

514 41.8 Ma), although subjected to pyritisation, have been identified as *Paralia sulcate*

515 and *Stephanopyxis turris*, the former common in coastal environments (McQuoid and

516 Nordberg, 2003) and the latter recognised as a shallow water coastal taxon (Mitlehner

517 and Hart, 2010). Thus, a more coastal and fluvially influenced depocentre for Site 913

518 before 39 Ma cannot be ruled out. Anomalously low fish apatite $\delta^{18}O$ values also

519 suggest that Site 913 was influenced by freshwater outflow, at least in the early

520 Eocene (Andreasson and Schmitz, 1996; Waddell and Moore, 2008). As such, the

521 high organic matter inputs of inferred fluvial origin in older sediments could have been

522 due to a wetter climate but also could reflect a more proximal location and depositional

523 environment related to the evolution of the basin.

524

525 **4.2.2. Glacial processes: an additional control on biomarker transport?**

526 As discussed above, not all biomarker secular trends can be readily explained by a

527 decrease in fluvial or constant/increasing aeolian inputs. In particular, increasing BIT

528 indices during the middle and late Eocene (~40 Ma onwards) are incompatible with an

529 inferred decrease in fluvial organic matter input. The very high BIT values observed in

530 some intervals (> 0.9) are also inconsistent with aeolian input or *in situ* production of

531 brGDGTs (Peterse et al., 2009; Weijers et al., 2014); as such, we suggest that these

532 high but variable BIT indices reflect an increase in periodic ice rafting as proposed by

533 Schouten et al. (2008). This interpretation is supported by the large and unexpected

534 input of thermally mature hopanoids after 40 Ma (Fig. 6a); we attribute this to glacial

535 erosion and reworking of sedimentary organic matter and transport via ice rafting, a

536 mechanism commonly invoked to explain changes in biomarker maturity within

537 Quaternary (Hefter et al., 2017; Parnell et al., 2007), Neogene (Duncan et al., 2019)

538 and late Paleogene (Duncan et al., 2019) marine sediments.

539   Although the regional glacial history of the Northern Hemisphere during the

540   Eocene is the subject of considerable debate, there is other evidence for cryospheric

541   development in the middle Eocene (~40 Ma onwards). This includes the presence of

542   ice rafted debris at ODP Site 913 (Eldrett et al., 2007), sea ice diatoms in the Arctic

543   (Moran et al., 2006; Stickley et al., 2009) and benthic foraminiferal $\delta^{18}O$ values (Tripati

544   et al., 2005 although this is disputed e.g. Edgar et al., 2007). Input of IRD at ODP Site

545   913 also coincides with a minimum in TEX_{86} SST estimates, strengthening the case

546   for a possible intermittent, localised glaciation.

547

548   **4.3   Leaf wax δ^2H values indicate an unstable high-latitude hydrological cycle**

549   Leaf wax δ^2H values provide an additional tool for exploring changes in the

550   hydrological cycle. The common δ^2H trends between C_{29} and C_{31} *n*-alkanes during the

551   early and late Eocene appear to be indicative of a climatic (rather than biosynthetic)

552   control. However, there is a significant offset between the C_{31} and C_{29} *n*-alkanes during

553   the middle Eocene (Fig. 6a), perhaps suggesting that these compounds are derived

554   from different plant species or sourced from regions with distinct climates within the

555   source region(s). We hypothesise that the C_{31} *n*-alkane, which is isotopically depleted

556   relative to the C_{29} *n*-alkane, could derive from mountainous regions, whereas the C_{29}

557   could derive from low-lying coastal plains. This *ad hoc* assumption arises from the ^2H-

558   depletion of around 25‰ expected for ~2000 m in the eastern Greenland mountains

559   relative to sea level for the modern day (based upon the Online Isotopes in

560   Precipitation Calculator; Bowen and Revenaugh et al., 2003). If the different records

561   do reflect different source regions, then this mechanism requires an explanation for

562   their convergence after ~40 Ma. This could be due to a simplification of sources arising

563   from the shift to solely aeolian inputs (as opposed to a more complex mixture of aeolian

564 and fluvial inputs; see above). It could also be due to upland glaciation preventing

565 vegetation cover on higher slopes, meaning that both the C_{29} and C_{31} *n*-alkanes are

566 sourced from more lowland regions from ~40 Ma onwards. This is consistent with

567 evidence from biomarkers (Schouten et al., 2008; this paper) and sedimentology

568 (Eldrett et al., 2009) which suggests ephemeral glaciation from ~40 Ma onwards.

569 Support for changing leaf wax inputs is also indicated by the decrease in *n*-alkane

570 ACLs in the later stages of the Eocene (Figure 3a).

571 Acknowledging the many assumptions in estimating them, the isotopic

572 composition of precipitation ($\delta^2 H_{precip}$; Figure 6b) can be estimated by assuming a net

573 fractionation factor (ε_{precip}) of 130‰, as in other Eocene studies (Pagani et al., 2006;

574 Handley et al., 2011; Handley et al., 2012). This yields an estimated Eocene $\delta^2 H_{precip}$

575 that is enriched relative to modern day values from the coastline of Greenland (Table

576 1). This assumed fractionation factor integrates a range of variables, including

577 evaporative enrichment (in soil and leaf), biosynthetic effects and plant type (Sachse

578 et al. 2012). These estimates also likely underestimate the difference between Eocene

579 and modern processes, because we do not correct for the absence of extensive

580 continental ice sheets in the Eocene; this would have caused global seawater (and

581 therefore precipitation source water) to be ^2H depleted rather than enriched relative to

582 modern, perhaps by ~8 - 12‰ (Tindall et al., 2010). There are several likely reasons

583 for Eocene precipitation $\delta^2 H$ values at ODP Site 913 to be enriched relative to those

584 of modern Greenland (-80 to -130‰; Table 1). Firstly, given the more southerly

585 location of the drill site, at around 65°N in the early Eocene (compared to ~75°N today),

586 the extent of Rayleigh distillation was likely lower (Dansgaard, 1964). Secondly,

587 warmer source waters yield more ^2H-enriched water vapour. This is consistent with

588 previous work on the PETM suggesting that under warmer climate conditions,

589 decreased rainout at mid-latitudes results in more ^{2}H-enriched precipitation at high

590 latitudes (Handley et al., 2011; Pagani et al., 2006).

	δ^2H_{precip} (‰)												
	Jan	Feb	Mar	Ap	May	Jun	July	Aug	Sept	Oct	Nov	Dec	Annual
(1) Shannon Island (75°N, 18°W)	-133	-129	-130	-130	-117	-109	-95	-96	-109	-126	-135	-137	-121
(2) Ittoqqortoormmit (71°N, 23°W)	-115	-110	-109	-107	-98	-93	-86	-85	-92	-106	-116	-118	-103
(3) Gunnbjorn (68°N, 30°W)	-100	-91	-94	-92	-85	-82	-82	-80	-81	-93	-101	-101	-91

Average inferred from Eocene leaf waxes: -100 to -20 ‰

591

592 **Table 1: Estimates of modern-day precipitation δ^2H_{precip} for locations on the**

593 **Greenland coast**. Estimates are derived from the Online Isotopes in Precipitation

594 Calculator (Bowen, 2016)

595   The temporal trends, however, are more difficult to interpret and both the C_{29}

596 and C_{31} n-alkanes indicate a secular shift towards higher δ^2H_{precip} values at a time of

597 global and regional cooling. Superficially, this appears to document an unexpected

598 increase in poleward moisture transport, occurring when Greenland was drifting

599 northwards and whilst regional temperatures were declining, i.e. in contrast to the

600 mechanisms and observations described above. Lower δ^2H_{precip} values during the

601 early Eocene could potentially be explained by an `amount effect' style response

602 (Dansgaard, 1964), whereby extensive airmass rainout results in a predominance of

603 ^{2}H-depleted precipitation. Although changes in the nature of mid-latitude precipitation

604 to more extreme, convective style storms has been invoked at the PETM to explain

605 geomorphological change in central US (Foreman et al., 2012) (paleolatitude ~42°N)

606 and on the northern Tethyan margin (Schmitz and Pujalte, 2007) (paleolatitude

607 ~38°N), whether this mechanism could be important at latitudes >60 °N remains

608 uncertain (e.g. Carmichael et al., 20187). However, Krishnan et al. (2014) observe a

609 ~15‰ δ^2H depletion during the onset of the ETM2 hyperthermal at Lomonosov Ridge

610 (Arctic Ocean), implying a larger 'amount effect'. Refinement of the Lomonosov ridge

611 age model has also resulted in suggestions that the enrichment described by Pagani

612 et al. (2006; see above) occurred ahead of the PETM warming, with more depleted

613 δ^2H values within the body of the PETM event. Extremely depleted δ^{18}O values within

614 dinosaur tooth enamel have also been reported for the mid-Cretaceous (Suarez et al.,

615 2013), argued to reflect high-latitude amount effects.

616 　　　In summary, leaf wax δ^2H values indicate enhanced poleward moisture

617 transport during the Eocene (relative to modern). This is consistent with PETM-aged

618 records (Carmichael et al., 2017 and ref. therein) and is attributed to enhanced

619 temperatures and a lower paleolatitude. However, the temporal trends are complex,

620 potentially reflecting changes in the source(s) of moisture associated with local

621 convective vs large scale circulation processes – and the magnitude of 'rainout' effects

622 associated with each. Of course, other factors such as changes in leaf wax source

623 (both in terms of vegetation and geography) cannot be precluded. These uncertainties

624 dictate caution when applying n-alkane δ^2H over very long timescales (e.g. $> 10^6$

625 years) but also in response to transient events (e.g. PETM), which are often

626 characterised by similar or smaller perturbations.

627

628 **4.4　Paleogeography and CO_2 influence the hydrological cycle on East**

629 **Greenland during the Eocene**

630 Multiple controls are likely to have influenced environmental changes on the

631 Greenland continent during the ~16 million years studied here. Within the ODP Site

632 913 record, this complexity is represented by a range of sometimes contradictory

633 climatic and environmental reconstructions. Here we apply climate model simulations

634 (HadCM3L) to explore the relative effects of CO_2 and paleogeography on mean annual

635 precipitation (MAP) near East Greenland. Simulations are performed for each

636 geological stage of the Eocene at 2x and 4x preindustrial CO_2 (560 ppmv and 1120

637 ppmv respectively; Fig 8).

638
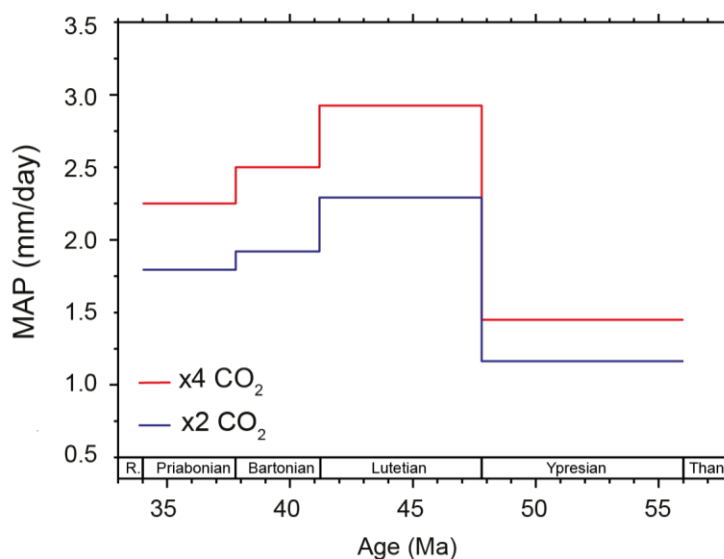
Figure 8: Model-simulated changes in hydrological cycle over continental Greenland for each stage of the Eocene. Mean annual precipitation shown for 4 x preindustrial CO_2 (red; 1120 ppmv) and 2 x preindustrial CO_2 (blue; 560 ppmv)

639

640 Model simulations indicate a reduction in MAP (ca. 25 and 30%) between the

641 x4 and x2 CO_2 simulations. This is observed for all four stages of the Eocene and

642 suggests that declining CO_2 during the middle and late Eocene (Anagnostou et al.,

643 2016) can account for the inferred decrease in terrigenous organic matter at ODP Site

644 913. Model simulations also indicate that paleogeography can exert an important

645 control on the hydrological cycle, with a gradual decrease in MAP (ca. 20-30%)

646 between the Lutetian (41.2 to 47.8 Ma) and Priabonian (37.8 to 34.0 Ma). This is also

647 consistent with the inferred decrease in terrigenous organic matter inputs at Site 913

648 during the middle and late Eocene. Intriguingly, the lowest MAP values are obtained

649 for the early Eocene simulations (i.e. during an interval which appears to have been

650 associated with an intensified hydrological cycle; e.g. Carmichael et al., 2016). The

651 reason for this remains unclear, however recent work has illustrated decoupling

652 between MAP and precipitation extremes occur during past warm climates (e.g. the

653 PETM), such that these two processes do not always change in the same sense as

654 each other (Carmichael et al., 2018).

655 Regardless, the model simulations suggest that both a decline in pCO$_2$ and

656 paleogeography likely caused weakening of precipitation (and terrestrial organic

657 matter inputs) during the middle and late Eocene. However, isotope-enabled

658 simulations which include hydrogen isotopes conducted with paleogeographic

659 reconstructions representative of the Eocene stages would prove useful for further

660 interrogating the data presented within this paper.

661

662 **5. Conclusions**

663 Biomarker abundances and distributions indicate changes in the source and transport

664 mechanisms of terrigenous organic matter from the Greenland continent to ODP Site

665 913 during the Eocene. In particular, a marked decline in the concentration of conifer-

666 derived diterpenoid and angiosperm-derived triterpenoid hydrocarbons during the

667 middle and late Eocene is suggested to reflect a declining influence of fluvial inputs.

668 Ice rafting could have been important after ~40 Ma, as indicated by a shift to more

669 variable BIT values and more mature hopane isomerisation parameters. This is

670 consistent with the previous identification of glacial dropstones and IRD at ~38 Ma and

671 indicates that thermally-mature lipid biomarkers could be a useful tool to help

672 fingerprint IRD in Paleogene marine sediments.

673   Although the biomarker distributions suggest weakening fluvial input from

674 Greenland in response to declining CO_2 and temperatures, the *n*-alkane δ^2H signal

675 suggests relatively ^2H-depleted values in the early Eocene. At face value, the

676 occurrence of isotopically depleted meteoric waters during the warmest interval,

677 apparent in both the C_{29} and C_{31} biomarkers, suggests that Rayleigh distillation was

678 not the primary control on Greenland precipitation. If this were the case, fundamentally

679 different controls on the high latitude hydrological cycle may have existed throughout

680 the early Eocene (e.g. high-latitude 'amount effects'). Critically, despite the range of

681 caveats, the new leaf wax δ^2H record and dramatic changes in biomarker abundances

682 suggest a far less stable hydrological cycle at the mid-high latitudes during the Eocene

683 than that suggested by the pollen record alone.

684

685 **Acknowledgements**

697

Contributions

699   G.N.I, M.C, D.L and R.D.P designed the study. G.N.I and M.C generated and

700   analysed organic geochemical data. A.F and D.L performed HadCM3L model

701   simulations. All authors contributed to data and model interpretations. G.N.I and

702   M.C. wrote the text, with input from all authors.

703

Competing interests

705   The authors declare no competing interests.

706

References

708   Anagnostou, E., John, E.H., Edgar, K.M., Foster, G.L., Ridgwell, A., Inglis, G.N.,

709   Pancost, R.D., Lunt, D.J. and Pearson, P.N. (2016) Changing atmospheric CO_2

710   concentration was the primary driver of early Cenozoic climate. *Nature* **533**,

711   380-384.

712   Andreasson, F.P. and Schmitz, B. (1996) Winter and summer temperatures of the

713   early middle Eocene of France from Turritella $\delta^{18}O$ profiles. *Geology* **24**, 1067-

714   1070.

715   Andreasson, F.P., Schmitz, B. and Spiegler, D. (1996) Stable isotopic composition

716   ($\delta^{18}O$, $\delta^{13}C$) of early Eocene fish-apatite from Hole 913B: An indicator of the

717   early Norwegian–Greenland Sea paleosalinity: in, Proceedings of the Ocean

718   Drilling Program, p. 583-591.

719   Baas, M., Pancost, R., van Geel, B. and Sinninghe Damsté, J.S. (2000) A

720   comparative study of lipids in *Sphagnum* species. *Organic Geochemistry* **31**,

721   535-541.

722   Beaulieu, E., Goddéris, Y., Donnadieu, Y., Labat, D. and Roelandt, C. (2012) High

723   sensitivity of the continental-weathering carbon dioxide sink to future climate

724   change. *Nature Climate Change* **2**, 346.

725   Bechtel, A., Sachsenhofer, R.F., Markic, M., Gratzer, R., Lücke, A. and Püttmann,

726   W. (2003) Paleoenvironmental implications from biomarker and stable isotope

727   investigations on the Pliocene Velenje lignite seam (Slovenia). *Organic*

728   *Geochemistry* **34**, 1277-1298.

729   Bice, K.L. and Marotzke, J. (2002) Could changing ocean circulation have

730   destabilized methane hydrate at the Paleocene/Eocene boundary?

731   *Paleoceanography & Paleoclimatology* **17**.

732   Bijl, P.K., Schouten, S., Sluijs, A., Reichart, G.-J., Zachos, J.C. and Brinkhuis, H.

733   (2009) Early Palaeogene temperature evolution of the southwest Pacific

734   Ocean. *Nature* **461**, 776-779.

735   Bowen, G.J. and Revenaugh, J. (2003) Interpolating the isotopic composition of

736   modern meteoric precipitation. *Water Resources Research* **39**.

737   Bray, E.E. and Evans, E.D. (1961) Distribution of *n*-paraffins as a clue to recognition

738   of source beds. *Geochimica et Cosmochimica Acta* **22**, 2-15.

739   Bush, R.T. and McInerney, F.A. (2013) Leaf wax *n*-alkane distributions in and across

740   modern plants: Implications for paleoecology and chemotaxonomy. *Geochimica*

741   *et Cosmochimica Acta* **117**, 161-179.

742   Carmichael, M.J., Inglis, G.N., Badger, M.P., Naafs, B.D.A., Behrooz, L.,

743   Remmelzwaal, S., Monteiro, F.M., Rohrssen, M., Farnsworth, A. and Buss, H.L.

744   (2017) Hydrological and associated biogeochemical consequences of rapid

745   global warming during the Paleocene-Eocene Thermal Maximum. *Global and*

746   *Planetary Change* **157**, 114-138.

747 Carmichael, M.J., Lunt, D.J., Huber, M., Heinemann, M., Kiehl, J., LeGrande, A.,

748   Loptson, C.A., Roberts, C.D., Sagoo, N. and Shields, C. (2016) A model–model

749   and data–model comparison for the early Eocene hydrological cycle. *Climate of*

750   *the Past* **12**, 455-481.

751 Carmichael, M.J., Pancost, R.D. and Lunt, D.J. (2018) Changes in the occurrence of

752   extreme precipitation events at the Paleocene–Eocene thermal maximum.

753   *Earth and Planetary Science Letters* **501**, 24-36.

754 Cramwinckel, M.J., Huber, M., Kocken, I.J., Agnini, C., Bijl, P.K., Bohaty, S.M.,

755   Frieling, J., Goldner, A., Hilgen, F.J. and Kip, E.L. (2018) Synchronous tropical

756   and polar temperature evolution in the Eocene. *Nature* **559**, 382.

757 Cranwell, P. (1982) Lipids of aquatic sediments and sedimenting particulates.

758   *Progress in Lipid Research* **21**, 271-308.

759 Crouch, E.M., Dickens, G.R., Brinkhuis, H., Aubry, M.-P., Hollis, C.J., Rogers, K.M.

760   and Visscher, H. (2003) The Apectodinium acme and terrestrial discharge

761   during the Paleocene–Eocene thermal maximum: new palynological,

762   geochemical and calcareous nannoplankton observations at Tawanui, New

763   Zealand. *Palaeogeography, Palaeoclimatology, Palaeoecology* **194**, 387-403.

764 Dansgaard, W. (1964) Stable isotopes in precipitation. *Tellus* **16**, 436-468.

765 De Jonge, C., Hopmans, E.C., Zell, C.I., Kim, J.-H., Schouten, S. and Sinninghe

766   Damsté, J.S. (2014) Occurrence and abundance of 6-methyl branched glycerol

767   dialkyl glycerol tetraethers in soils: Implications for palaeoclimate

768   reconstruction. *Geochimica et Cosmochimica Acta* **141**, 97-112.

769 de Las Heras, F., Grimalt, J. and Albaigés, J. (1991) Novel C-ring cleaved

770   triterpenoid-derived aromatic hydrocarbons in Tertiary brown coals. *Geochimica*

771   *et Cosmochimica Acta* **55**, 3379-3385.

772 Diefendorf, A.F., Freeman, K.H. and Wing, S.L. (2012) Distribution and carbon

773   isotope patterns of diterpenoids and triterpenoids in modern temperate C_3 trees

774   and their geochemical significance. *Geochimica et Cosmochimica Acta* **85**,

775   342-356.

776 Diefendorf, A.F., Freeman, K.H. and Wing, S.L. (2014) A comparison of terpenoid

777   and leaf fossil vegetation proxies in Paleocene and Eocene Bighorn Basin

778   sediments. *Organic Geochemistry* **71**, 30-42.

779 Diefendorf, A.F., Freeman, K.H., Wing, S.L. and Graham, H.V. (2011) Production of

780   *n*-alkyl lipids in living plants and implications for the geologic past. *Geochimica*

781   *et Cosmochimica Acta* **75**, 7472-7485.

782 Diefendorf, A.F. and Freimuth, E.J. (2017) Extracting the most from terrestrial plant-

783   derived *n*-alkyl lipids and their carbon isotopes from the sedimentary record: A

784   review. *Organic Geochemistry* **103**, 1-21.

785 Duncan, B., McKay, R., Bendle, J., Naish, T., Inglis, G.N., Moossen, H., Levy, R.,

786   Ventura, G.T., Lewis, A. and Chamberlain, B. (2019) Lipid biomarker

787   distributions in Oligocene and Miocene sediments from the Ross Sea region,

788   Antarctica: Implications for use of biomarker proxies in glacially-influenced

789   settings. *Palaeogeography, Palaeoclimatology, Palaeoecology* **516**, 71-89.

790 Dypvik, H., Riber, L., Burca, F., Rüther, D., Jargvoll, D., Nagy, J. and Jochmann, M.

791   (2011) The Paleocene–Eocene thermal maximum (PETM) in Svalbard—clay

792   mineral and geochemical signals. *Palaeogeography, Palaeoclimatology,*

793   *Palaeoecology* **302**, 156-169.

794   Edgar, K.M., Wilson, P.A., Sexton, P.F. and Suganuma, Y. (2007) No extreme

795   bipolar glaciation during the main Eocene calcite compensation shift. *Nature*

796   **448**, 908.

797   Eglinton, G. and Hamilton, R.J. (1967) Leaf Epicuticular Waxes. *Science* **156**, 1322-

798   1335.

799   Eglinton, T., Eglinton, G., Dupont, L., Sholkovitz, E., Montluçon, D. and Reddy, C.

800   (2002) Composition, age, and provenance of organic matter in NW African dust

801   over the Atlantic Ocean. *Geochemistry, Geophysics, Geosystems* **3**, 1-27.

802   Eldrett, J.S., Greenwood, D.R., Harding, I.C. and Huber, M. (2009) Increased

803   seasonality through the Eocene to Oligocene transition in northern high

804   latitudes. *Nature* **459**, 969-973.

805   Eldrett, J.S., Harding, I.C., Wilson, P.A., Butler, E. and Roberts, A.P. (2007)

806   Continental ice in Greenland during the Eocene and Oligocene. *Nature* **446**,

807   176-179.

808   Farnsworth, A., Lunt, D.J., O'Brien, C., Foster, G.L., Inglis, G.N., Markwick, P.,

809   Pancost, R.D. and Robinson, S. (In Revision) Climate sensitivity on geological

810   timescales controlled by non-linear feedbacks and ocean circulation.

811   *Geophysical Research Letters*.

812   Ficken, K., Li, B., Swain, D. and Eglinton, G. (2000) An *n*-alkane proxy for the

813   sedimentary input of submerged/floating freshwater aquatic macrophytes.

814   *Organic Geochemistry* **31**, 745-749.

815   Foreman, B.Z., Heller, P.L. and Clementz, M.T. (2012) Fluvial response to abrupt

816   global warming at the Palaeocene/Eocene boundary. *Nature* **491**, 92-95.

817   Garel, S., Schnyder, J., Jacob, J., Dupuis, C., Boussafir, M., Le Milbeau, C., Storme,

818   J.-Y., Iakovleva, A.I., Yans, J., Baudin, F., Fléhoc, C. and Quesnel, F. (2013)

819   Paleohydrological and paleoenvironmental changes recorded in terrestrial

820   sediments of the Paleocene–Eocene boundary (Normandy, France).

821   *Palaeogeography, Palaeoclimatology, Palaeoecology* **376**, 184-199.

822 Handley, L., Crouch, E.M. and Pancost, R.D. (2011) A New Zealand record of sea

823   level rise and environmental change during the Paleocene–Eocene Thermal

824   Maximum. *Palaeogeography, Palaeoclimatology, Palaeoecology* **305**, 185-200.

825 Handley, L., O'Halloran, A., Pearson, P.N., Hawkins, E., Nicholas, C.J., Schouten,

826   S., McMillan, I.K. and Pancost, R.D. (2012) Changes in the hydrological cycle

827   in tropical East Africa during the Paleocene–Eocene Thermal Maximum.

828   *Palaeogeography, Palaeoclimatology, Palaeoecology* **329**, 10-21.

829 Hefter, J., Naafs, B.D.A. and Zhang, S. (2017) Tracing the source of ancient

830   reworked organic matter delivered to the North Atlantic Ocean during Heinrich

831   Events. *Geochimica et Cosmochimica Acta* **205**, 211-225.

832 Held, I.M. and Soden, B.J. (2006) Robust responses of the hydrological cycle to

833   global warming. *Journal of Climate* **19**, 5686-5699.

834 Hohbein, M.W., Sexton, P.F. and Cartwright, J.A. (2013) Onset of North Atlantic

835   Deep Water production coincident with inception of the Cenozoic global cooling

836   trend. *Geology* **40**, 255-258

837 Hollis, C.J., Dunkley Jones, T., Anagnostou, E., Bijl, P.K., Cramwinckel, M.J., Cui,

838   Y., Dickens, G.R., Edgar, K.M., Eley, Y., Evans, D., Foster, G.L., Frieling, J.,

839   Inglis, G.N., Kennedy, E.M., Kozdon, R., Lauretano, V., Lear, C.H., Littler, K.,

840   Meckler, N., Naafs, B.D.A., Pälike, H., Pancost, R.D., Pearson, P., Royer, D.L.,

841   Salzmann, U., Schubert, B., Seebeck, H., Sluijs, A., Speijer, R., Stassen, P.,

842   Tierney, J., Tripati, A., Wade, B., Westerhold, T., Witkowski, C., Zachos, J.C.,

843   Zhang, Y.G., Huber, M. and Lunt, D.J. (2019) The DeepMIP contribution to

844   PMIP4: methodologies for selection, compilation and analysis of latest

845   Paleocene and early Eocene climate proxy data, incorporating version 0.1 of

846   the DeepMIP database. *Geosci. Model Dev. Discuss.* **2019**, 1-98.

847 Hopmans, E.C., Schouten, S. and Damsté, J.S.S. (2016) The effect of improved

848   chromatography on GDGT-based palaeoproxies. *Organic Geochemistry* **93**, 1-

849   6.

850 Hopmans, E.C., Weijers, J.W., Schefuß, E., Herfort, L., Sinninghe Damsté, J.S. and

851   Schouten, S. (2004) A novel proxy for terrestrial organic matter in sediments

852   based on branched and isoprenoid tetraether lipids. *Earth and Planetary*

853   *Science Letters* **224**, 107-116.

854 Inglis, G.N., Collinson, M.E., Riegel, W., Wilde, V., Robson, B.E., Lenz, O.K. and

855   Pancost, R.D. (2015a) Ecological and biogeochemical change in an early

856   Paleogene peat-forming environment: Linking biomarkers and palynology.

857   *Palaeogeography, Palaeoclimatology, Palaeoecology* **438**, 245-255.

858 Inglis, G.N., Farnsworth, A., Lunt, D., Foster, G.L., Hollis, C.J., Pagani, M., Jardine,

859   P.E., Pearson, P.N., Markwick, P., Galsworthy, A.M.J., Raynham, L., Taylor,

860   K.W.R. and Pancost, R.D. (2015b) Descent toward the Icehouse: Eocene sea

861   surface cooling inferred from GDGT distributions. *Paleoceanography* **30**, 1000-

862   1020.

863 Inglis, G.N., Naafs, B.D.A., Zheng, Y., McClymont, E.L., Evershed, R.P. and

864   Pancost, R.D. (2018) Distributions of geohopanoids in peat: Implications for the

865   use of hopanoid-based proxies in natural archives. *Geochimica et*

866   *Cosmochimica Acta* **224**, 249-261.

867 Jacob, J., Disnar, J.-R., Boussafir, M., Spadano Albuquerque, A.L., Sifeddine, A. and

868   Turcq, B. (2007) Contrasted distributions of triterpene derivatives in the

869   sediments of Lake Caçó reflect paleoenvironmental changes during the last

870   20,000 yrs in NE Brazil. *Organic Geochemistry* **38**, 180-197.

871 Kelly, D.C., Zachos, J.C., Bralower, T.J. and Schellenberg, S.A. (2005) Enhanced

872   terrestrial weathering/runoff and surface ocean carbonate production during the

873   recovery stages of the Paleocene-Eocene thermal maximum.

874   *Paleoceanography* **20**.

875 Kender, S., Stephenson, M.H., Riding, J.B., Leng, M.J., Knox, R.W.B., Peck, V.L.,

876   Kendrick, C.P., Ellis, M.A., Vane, C.H. and Jamieson, R. (2012) Marine and

877   terrestrial environmental changes in NW Europe preceding carbon release at

878   the Paleocene–Eocene transition. *Earth and Planetary Science Letters* **353**,

879   108-120.

880 Kennett, J.P. and Stott, L.D. (1991) Abrupt Deep-Sea Warming, Palaeoceanographic

881   Changes and Benthic Extinctions at the End of the Paleocene. *Nature* **353**,

882   225-229.

883 Kim, J.-H., Van der Meer, J., Schouten, S., Helmke, P., Willmott, V., Sangiorgi, F.,

884   Koç, N., Hopmans, E.C. and Damsté, J.S.S. (2010) New indices and

885   calibrations derived from the distribution of crenarchaeal isoprenoid tetraether

886   lipids: Implications for past sea surface temperature reconstructions.

887   *Geochimica et Cosmochimica Acta* **74**, 4639-4654.

888 Krishnan, S., Pagani, M., Huber, M. and Sluijs, A. (2014) High latitude hydrological

889   changes during the Eocene Thermal Maximum 2. *Earth and Planetary Science*

890   *Letters* **404**, 167-177.

891 Lin, H.-C. and Chang, W.-L. (2000) Diterpenoids from Salvia miltiorrhiza.

892   *Phytochemistry* **53**, 951-953.

893 Mackenzie, A., Patience, R., Maxwell, J., Vandenbroucke, M. and Durand, B. (1980)

894   Molecular parameters of maturation in the Toarcian shales, Paris Basin,

895   France—I. Changes in the configurations of acyclic isoprenoid alkanes,

896   steranes and triterpanes. *Geochimica et Cosmochimica Acta* **44**, 1709-1721.

897 McQuoid, M.R. and Nordberg, K. (2003) The diatom Paralia sulcata as an

898   environmental indicator species in coastal sediments. *Estuarine, Coastal and*

899   *Shelf Science* **56**, 339-354.

900 Medeiros, P.M., Sikes, E.L., Thomas, B. and Freeman, K.H. (2012) Flow discharge

901   influences on input and transport of particulate and sedimentary organic carbon

902   along a small temperate river. *Geochimica et Cosmochimica Acta* **77**, 317-334.

903 Medeiros, P.M. and Simoneit, B.R. (2008) Multi-biomarker characterization of

904   sedimentary organic carbon in small rivers draining the Northwestern United

905   States. *Organic Geochemistry* **39**, 52-74.

906 Mitlehner, A. and Hart, M. (2010) The discovery of a Middle Eocene diatom flora

907   from Whitecliff Bay, Isle of Wight England. *Micropalaeontology, Sedimentary*

908   *Environments and Stratigraphy: A Tribute to Dennis Curry*, 217-233.

909 Moran, K., Backman, J., Brinkhuis, H., Clemens, S.C., Cronin, T., Dickens, G.R.,

910   Eynaud, F., Gattacceca, J., Jakobsson, M. and Jordan, R.W. (2006) The

911   Cenozoic palaeoenvironment of the Arctic Ocean. *Nature* **441**, 601.

912 Myhre, A., Thiede, J. and Firth, J. (1995) Shipboard Scientific Party, Initial Reports:

913   sites 907–913, North Atlantic-Arctic Gateways. *Proceedings, Initial Reports,*

914   *Ocean Drilling Program* **151**, 926.

915 Naafs, B., Gallego-Sala, A., Inglis, G. and Pancost, R. (2017) Refining the global

916   branched glycerol dialkyl glycerol tetraether (brGDGT) soil temperature

917   calibration. *Organic Geochemistry* **106**, 48-56.

918   Nakamura, H., Sawada, K. and Takahashi, M. (2010) Aliphatic and aromatic

919   terpenoid biomarkers in Cretaceous and Paleogene angiosperm fossils from

920   Japan. *Organic Geochemistry* **41**, 975-980.

921   Nott, C.J., Xie, S., Avsejs, L.A., Maddy, D., Chambers, F.M. and Evershed, R.P.

922   (2000) n-Alkane distributions in ombrotrophic mires as indicators of vegetation

923   change related to climatic variation. *Organic Geochemistry* **31**, 231-235.

924   Otto, A. and Simoneit, B.R.T. (2001) Chemosystematics and diagenesis of

925   terpenoids in fossil conifer species and sediment from the Eocene Zeitz

926   formation, Saxony, Germany. *Geochimica et Cosmochimica Acta* **65**, 3505-

927   3527.

928   Pagani, M., Pedentchouk, N., Huber, M., Sluijs, A., Schouten, S., Brinkhuis, H.,

929   Damsté, J.S.S., Dickens, G.R., Backman, J. and Clemens, S. (2006) Arctic

930   hydrology during global warming at the Palaeocene/Eocene thermal maximum.

931   *Nature* **442**, 671-675.

932   Pancost, R.D. and Boot, C.S. (2004) The palaeoclimatic utility of terrestrial

933   biomarkers in marine sediments. *Marine Chemistry* **92**, 239-261.

934   Pancost, R.D., Coleman, J.M., Love, G.D., Chatzi, A., Bouloubassi, I. and Snape,

935   C.E. (2008) Kerogen-bound glycerol dialkyl tetraether lipids released by

936   hydropyrolysis of marine sediments: A bias against incorporation of

937   sedimentary organisms? *Organic Geochemistry* **39**, 1359-1371.

938   Parnell, J., Bowden, S., Andrews, J.T. and Taylor, C. (2007) Biomarker

939   determination as a provenance tool for detrital carbonate events (Heinrich

940   events?): Fingerprinting Quaternary glacial sources into Baffin Bay. *Earth and*

941   *Planetary Science Letters* **257**, 71-82.

942   Peterse, F., Kim, J.-H., Schouten, S., Kristensen, D.K., Koç, N. and Sinninghe

943   Damsté, J.S. (2009) Constraints on the application of the MBT/CBT

944   palaeothermometer at high latitude environments (Svalbard, Norway). *Organic*

945   *Geochemistry* **40**, 692-699.

946   Pierrehumbert, R.T. (2002) The hydrologic cycle in deep-time climate problems.

947   *Nature* **419**, 191-198.

948   Rullkötter, J., Peakman, T.M. and Ten Haven, H. (1994) Early diagenesis of

949   terrigenous triterpenoids and its implications for petroleum geochemistry.

950   *Organic Geochemistry* **21**, 215-233.

951   Sachse, D., Billault, I., Bowen, G.J., Chikaraishi, Y., Dawson, T.E., Feakins, S.J.,

952   Freeman, K.H., Magill, C.R., McInerney, F.A. and Van der Meer, M.T. (2012)

953   Molecular paleohydrology: interpreting the hydrogen-isotopic composition of

954   lipid biomarkers from photosynthesizing organisms. *Annual Review of Earth*

955   *and Planetary Sciences*.

956   Sáenz, J.P., Grosser, D., Bradley, A.S., Lagny, T.J., Lavrynenko, O., Broda, M. and

957   Simons, K. (2015) Hopanoids as functional analogues of cholesterol in bacterial

958   membranes. *Proceedings of the National Academy of Sciences* **112**, 11971-

959   11976.

960   Schefuß, E., Schouten, S. and Schneider, R.R. (2005) Climatic controls on central

961   African hydrology during the past 20,000 years. *Nature* **437**, 1003.

962   Scherer, R.P. and Koç, N. (1996) Late Paleogene diatom biostratigraphy and

963   paleoenvironments of the northern Norwegian-Greenland Sea. *Proceedings of*

964   *the Ocean Drilling Program, Scientific Results, Vol. 151*.

965   Schmitz, B. and Pujalte, V. (2007) Abrupt increase in seasonal extreme precipitation

966   at the Paleocene-Eocene boundary. *Geology* **35**, 215-218.

967 Schouten, S., Eldrett, J., Greenwood, D.R., Harding, I., Baas, M. and Damsté, J.S.S.

968   (2008) Onset of long-term cooling of Greenland near the Eocene-Oligocene

969   boundary as revealed by branched tetraether lipids. *Geology* **36**, 147-150.

970 Schouten, S., Hopmans, E.C., Schefuß, E. and Sinninghe Damsté, J.S. (2002)

971   Distributional variations in marine crenarchaeotal membrane lipids: a new tool

972   for reconstructing ancient sea water temperatures? *Earth and Planetary*

973   *Science Letters* **204**, 265-274.

974 Sessions, A.L., Burgoyne, T.W. and Hayes, J.M. (2001) Determination of the H3

975   factor in hydrogen isotope ratio monitoring mass spectrometry. *Analytical*

976   *Chemistry* **73**, 200-207.

977 Sessions, A.L., Burgoyne, T.W., Schimmelmann, A. and Hayes, J.M. (1999)

978   Fractionation of hydrogen isotopes in lipid biosynthesis. *Organic Geochemistry*

979   **30**, 1193-1200.

980 Simoneit, B.R. (1977) Organic matter in eolian dusts over the Atlantic Ocean. *Marine*

981   *Chemistry* **5**, 443-464.

982 Simoneit, B.R.T., Grimalt, J.O., Wang, T.G., Cox, R.E., Hatcher, P.G. and

983   Nissenbaum, A. (1986) Cyclic terpenoids of contemporary resinous plant

984   detritus and of fossil woods, ambers and coals. *Organic Geochemistry* **10**, 877-

985   889.

986 Sinninghe Damsté, J.S., Rijpstra, W.I.C., Foesel, B.U., Huber, K.J., Overmann, J.,

987   Nakagawa, S., Kim, J.J., Dunfield, P.F., Dedysh, S.N. and Villanueva, L. (2018)

988   An overview of the occurrence of ether-and ester-linked iso-diabolic acid

989   membrane lipids in microbial cultures of the Acidobacteria: Implications for

990   brGDGT paleoproxies for temperature and pH. *Organic Geochemistry* **124**, 63-

991   76.

992   Sluijs, A., Bowen, G., Brinkhuis, H., Lourens, L. and Thomas, E. (2007) The

993   Palaeocene-Eocene Thermal Maximum super greenhouse: biotic and

994   geochemical signatures, age models and mechanisms of global change. *Deep*

995   *Time Perspectives on Climate Change: Marrying the Signal From Computer*

996   *Models and Biological Proxies*, 323-347.

997   Sluijs, A., Röhl, U., Schouten, S., Brumsack, H.-J., Sangiorgi, F., Sinninghe Damsté,

998   J.S. and Brinkhuis, H. (2008) Arctic late Paleocene–early Eocene

999   paleoenvironments with special emphasis on the Paleocene-Eocene thermal

1000   maximum (Lomonosov Ridge, Integrated Ocean Drilling Program Expedition

1001   302). *Paleoceanography* **23**, PA1S11.

1002   Sluijs, A., Schouten, S., Pagani, M., Woltering, M., Brinkhuis, H., Damste, J.S.S.,

1003   Dickens, G.R., Huber, M., Reichart, G.J., Stein, R., Matthiessen, J., Lourens,

1004   L.J., Pedentchouk, N., Backman, J., Moran, K. and Scientists, E. (2006)

1005   Subtropical arctic ocean temperatures during the Palaeocene/Eocene thermal

1006   maximum. *Nature* **441**, 610-613.

1007   Smith, F., Wing, S. and Freeman, K. (2007) Carbon and hydrogen isotope

1008   compositions of plant lipids during the PETM as evidence for the response of

1009   terrestrial ecosystems to rapid climate change. *Earth and Planetary Science*

1010   *Letters* **262**, 50-65.

1011   Stickley, C.E., St John, K., Koç, N., Jordan, R.W., Passchier, S., Pearce, R.B. and

1012   Kearns, L.E. (2009) Evidence for middle Eocene Arctic sea ice from diatoms

1013   and ice-rafted debris. *Nature* **460**, 376-379.

1014   Suarez, C.A., Ludvigson, G., Gonzalez, L., Fiorillo, A., Flaig, P. and McCarthy, P.

1015   (2013) Use of multiple oxygen isotope proxies for elucidating Arctic Cretaceous

palaeo-hydrology. *Geological Society, London, Special Publications* **382**, SP382. 383.

Talbot, H.M. and Farrimond, P. (2007) Bacterial populations recorded in diverse sedimentary biohopanoid distributions. *Organic Geochemistry* **38**, 1212-1225.

Thiede, J. and Myhre, A.M. (1996) 36. The palaeoceanographic history of the North Atlantic–Arctic gateways: synthesis of the Leg 151 drilling results, Proceedings of the Ocean Drilling Program, Scientific Results. Ocean Drilling Program College Station, TX, pp. 645-658.

Tierney, J.E., Russell, J.M., Huang, Y., Damsté, J.S.S., Hopmans, E.C. and Cohen, A.S. (2008) Northern hemisphere controls on tropical southeast African climate during the past 60,000 years. *Science* **322**, 252-255.

Tierney, J.E. and Tingley, M.P. (2014a) A Bayesian, spatially-varying calibration model for the TEX$_{86}$ proxy. *Geochimica et Cosmochimica Acta* **127**, 83-106.

Tierney, J.E. and Tingley, M.P. (2014b) A Bayesian, spatially-varying calibration model for the TEX$_{86}$ proxy. *Geochimica et Cosmochimica Acta* **127**, 83-106.

Tierney, J.E. and Tingley, M.P. (2015) A TEX$_{86}$ surface sediment database and extended Bayesian calibration. *Scientific data* **2**.

Tindall, J., Flecker, R., Valdes, P., Schmidt, D.N., Markwick, P. and Harris, J. (2010) Modelling the oxygen isotope distribution of ancient seawater using a coupled ocean–atmosphere GCM: implications for reconstructing early Eocene climate. *Earth and Planetary Science Letters* **292**, 265-273.

Tipple, B.J. and Pagani, M. (2010) A 35Myr North American leaf-wax compound-specific carbon and hydrogen isotope record: implications for C 4 grasslands and hydrologic cycle dynamics. *Earth and Planetary Science Letters* **299**, 250-262.

1041 Tipple, B.J., Pagani, M., Krishnan, S., Dirghangi, S.S., Galeotti, S., Agnini, C.,

1042   Giusberti, L. and Rio, D. (2011) Coupled high-resolution marine and terrestrial

1043   records of carbon and hydrologic cycles variations during the Paleocene–

1044   Eocene Thermal Maximum (PETM). *Earth and Planetary Science Letters* **311**,

1045   82-92.

1046 Tripati, A., Backman, J., Elderfield, H. and Ferretti, P. (2005) Eocene bipolar

1047   glaciation associated with global carbon cycle changes. *Nature* **436**, 341.

1048 Tripati, A. and Elderfield, H. (2005) Deep-sea temperature and circulation changes at

1049   the Paleocene-Eocene thermal maximum. *Science* **308**, 1894-1898.

1050 Vogts, A., Schefuß, E., Badewien, T. and Rullkötter, J. (2012) *n*-Alkane parameters

1051   from a deep sea sediment transect off southwest Africa reflect continental

1052   vegetation and climate conditions. *Organic Geochemistry* **47**, 109-119.

1053 Waddell, L.M. and Moore, T.C. (2008) Salinity of the Eocene Arctic Ocean from

1054   oxygen isotope analysis of fish bone carbonate. *Paleoceanography* **23**.

1055 Weijers, J.W., Schouten, S., van den Donker, J.C., Hopmans, E.C. and Sinninghe

1056   Damsté, J.S. (2007) Environmental controls on bacterial tetraether membrane

1057   lipid distribution in soils. *Geochimica et Cosmochimica Acta* **71**, 703-713.

1058 Weijers, J.W.H., Schefuß, E., Kim, J.-H., Sinninghe Damsté, J.S. and Schouten, S.

1059   (2014) Constraints on the sources of branched tetraether membrane lipids in

1060   distal marine sediments. *Organic Geochemistry* **72**, 14-22.

1061 White, T., González, L., Ludvigson, G. and Poulsen, C. (2001) Middle Cretaceous

1062   greenhouse hydrologic cycle of North America. *Geology* **29**, 363-366.

1063 Zachos, J.C., Dickens, G.R. and Zeebe, R.E. (2008) An early Cenozoic perspective

1064   on greenhouse warming and carbon-cycle dynamics. *Nature* **451**, 279-283.

1065 Zachos, J.C., Schouten, S., Bohaty, S., Quattlebaum, T., Sluijs, A., Brinkhuis, H.,

1066   Gibbs, S.J. and Bralower, T.J. (2006) Extreme warming of mid-latitude coastal

1067   ocean during the Paleocene-Eocene Thermal Maximum: Inferences from

1068   TEX86 and isotope data. *Geology* **34**, 737-740.

1069 Zachos, J.C., Wara, M.W., Bohaty, S., Delaney, M.L., Petrizzo, M.R., Brill, A.,

1070   Bralower, T.J. and Premoli-Silva, I. (2003) A transient rise in tropical sea

1071   surface temperature during the Paleocene-Eocene Thermal Maximum. *Science*

1072   **302**, 1551-1554.

1073